Earth and Planetary Science Letters 495 (2018) 112–134

Contents lists available at ScienceDirect

Earth and Planetary Science Letters

www.elsevier.com/locate/epsl

Frontiers

The geophysics, geology and mechanics of slow fault slip

Roland Bürgmann

Department of Earth and Planetary Science and Berkeley Seismology Lab, University of California, Berkeley, CA 94708, USA

ARTICLE INFO

Article history:
Received 16 February 2018
Received in revised form 30 April 2018
Accepted 30 April 2018
Available online xxxx
Editor: A. Yin

Keywords:
fault mechanics
slow earthquake
afterslip
friction
rheology
tremor

ABSTRACT

Modern geodetic and seismologic observations describe the behavior of fault slip over a vast range of spatial and temporal scales. Slip at sub-seismogenic speeds is evident from top to bottom of lithospheric faults and plays an important role throughout the earthquake cycle. Where earthquakes and tremor accompany slow slip, they help illuminate the spatiotemporal evolution of fault slip. Geophysical subsurface imaging and geologic field studies provide information about suitable environments of slow slip. In particular, exhumed fault and shear zones from various depths reveal the importance of multiple deformation processes and fault-zone structures. Most geologic examples feature frictionally weak and velocity-strengthening materials, well-developed mineral fabrics, and abundant veining indicative of near-lithostatic fluid pressure. To produce transient slow slip events and tremor, in addition to the presence of high-pressure fluids a heterogeneous fault-zone structure, composition, and/or metamorphic assemblage may be needed. Laboratory and computational models suggest that velocity-weakening slip patches smaller than a critical dimension needed for earthquake nucleation will also fail in slow slip events. Changes in fluid pressure or slip rate can cause a fault to transition between stable and unstable fault slip behavior. Future interdisciplinary investigations of slow fault slip, directly integrating geophysical, geological and modeling investigations, will further improve our understanding of the dynamics of slow slip and aid in providing more accurate earthquake hazard characterizations.

1. Introduction

Faults represent displacement discontinuities in rocks that accommodate lithospheric deformation by fast (seismic) and slower (aseismic) slip (Fig. 1). While earthquakes involve fault slip velocities ranging from 10^{-4} to 1 m/s and produce high-frequency seismic waves, slow slip, also referred to as fault creep, can be many orders of magnitude slower. However, there is no sharp boundary between the two modes of slip, and slow slip can sometimes involve radiation of long-period seismic energy or secondary small seismic events in the fault zone. The slip behavior on a fault may vary spatially and we refer to a fault that accommodates a fraction of its slip aseismically as partially coupled. The fault creep rate can be steady or vary in time. We refer to distinct episodes of accelerated slip as slow slip events (SSEs), creep events and slow (or silent) earthquakes. Slip duration at a point on a fault during an earthquake is generally less than ∼10 s, while an SSE may endure from tens of seconds to tens of years.

For a fault to slip slowly requires a strengthening mechanism that puts on the brakes and contains fault slip velocities to sub-seismogenic speeds. Independent of the process and physics involved, we refer to an increase of fault strength with rising slip rate as velocity strengthening, preventing fast earthquake rupture and promoting fault creep. Faults that weaken as slip rate increases are velocity weakening and may accelerate into a seismic stick-slip event or may limit themselves to produce an SSE if the elastic load stress decays more rapidly during slip than the strength of the fault. Whether fault offset occurs by a seismic or slow mode of slip appears to depend on the make-up of fault materials, the fault's environmental conditions, and the history and rate of loading. As geophysical observations improve, we find increasing evidence of slow slip in a wide range of tectonic regimes, fault environments and phases of the earthquake cycle of large ruptures. These observations and fault mechanical models also point to substantial complexity in fault behavior, including spatiotemporal transitions between slip modes. This has led to increased efforts in examining the geophysics, geology and mechanics of slow slip, in recent years.

Slow slip plays an important role in the earthquake cycle and associated earthquake hazard. If faults accommodate a substantial portion of their slip budget by slow slip, their seismic hazard is reduced. Observations of precursory SSEs and associated foreshocks suggest that accelerated creep can initiate or trigger some seismic events. While in no way universal, these observations have renewed interest in precursory activity and suggest the possibility

E-mail address: burgmann@berkeley.edu.

https://doi.org/10.1016/j.epsl.2018.04.062
0012-821X/

Table 1
Glossary of terms.

Afterslip	Post-earthquake slow slip on nearby fault sections relieving static coseismic stress change and decaying (~logarithmically) with time.
Cataclasite	Fault rock sheared by brittle fracturing and comminution of mineral grains.
Earthquake swarm	Burst of earthquakes that does not exhibit clear mainshock–aftershock pattern.
Fault coupling	The degree to which slip on a fault is accommodated by seismic vs. aseismic slip. Average coupling during an observation period can be expressed as a ratio ranging from <0 (accelerated creep), 0 (creep at long-term slip rate), 1 (fully locked), and >1 (creep opposite to long-term slip direction) (Wang and Dixon, 2004).
Fault gouge	Fine-grained, highly sheared fault zone material made of cataclasite that may also be chemically altered.
Low-frequency earthquake (LFE)	Small ($M_w \ll 3$) and short (<1 s) seismic events contained in more enduring tremor signal indicative of shear slip (Beroza and Ide, 2011).
Magnetotellurics (MT)	Geophysical imaging of lithospheric electrical conductivity structure using natural electromagnetic field variations as sources.
Mélange shear zone	Fault zone structure with heterogeneous mechanical properties comprising blocks of variable composition in sheared sedimentary matrix.
Mylonite	Foliated fault zone rock sheared by crystal plastic deformation mechanisms at high temperatures.
Rate and state friction	Empirical expressions describing the experimentally observed (logarithmic) dependence of frictional strength on slip velocity (rate) and an evolving time-dependent effect (state) (Marone, 1998).
Receiver function analysis	Characterization of body-wave scattering from teleseismic events to obtain a point measurement of crustal seismic velocity structure beneath a seismic station.
Repeating earthquakes	Earthquakes with nearly identical seismic waveforms, locations and mechanisms inferred to re-slip the same rupture surface, often driven by surrounding slow slip.
Slow slip (also aseismic slip and fault creep)	Fault slip that is slow enough to not produce seismic energy associated with earthquakes.
Slow slip event (SSE) (also creep event and slow/silent earthquake)	Aseismic slip transient on a fault patch over durations ranging from minutes to decades. Some slow earthquakes generate low-frequency seismic energy.
Tectonic tremor	Enduring low-frequency seismic signals generally interpreted as being associated with otherwise slow slip.
Triggered SSE	Slow slip episode following an earthquake due to static or dynamic stress changes that is not afterslip.
Very-low-frequency earthquake (VLFE)	Similar to LFEs but longer (10–200 s) and larger (M 3–4) seismic events generally associated with tremor (Beroza and Ide, 2011).

of raising hazard warning levels at times of accelerated slow slip. Transient slow slip relieving stress increases from recent earthquake ruptures on nearby fault sections is called afterslip. Static stress changes or dynamic shaking from earthquakes may also lead to triggered SSEs of any size, both near and very far from a mainshock. Postseismic slow slip of either kind helps expand the reach of stress interactions from an earthquake and may play an important role in the generation of aftershocks and extended sequences of hazardous earthquakes.

There are many excellent recent review papers on various aspects of slow slip. Schwartz and Rokosky (2007), Rubinstein et al. (2010), and Beroza and Ide (2011) focus on geophysical observations and the setting, properties and mechanics of episodic tremor and slip events below the base of the seismogenic zone. Peng and Gomberg (2010) and Schwartz (2015) highlight the wide spectrum of episodic slow slip characteristics. Obara and Kato (2016) relate slow earthquakes to large seismic ruptures, consider their similarities and differences, and emphasize the role that SSEs can have in the initiation of some great earthquakes. Wang and Bilek (2014) consider the role of seafloor morphology and other factors in the coupling of subduction thrusts around the world. Audet and Kim (2016) review insights gained from seismic imaging of deep-seated slow slip zones on subduction thrusts, while Saffer and Wallace (2015) examine the nature and environment of very shallow subduction slip episodes. Avouac (2015) puts slow slip in the context of the earthquake cycle, considering kinematic and dynamic models of the release of elastic strain energy by seismic and aseismic slip on mechanically heterogeneous faults. While many of these reviews were especially focused on subduction zones, Harris (2017) addresses the role of aseismic fault creep on shallow continental faults and examines to what degree slow slip changes the character of large earthquakes on partially coupled faults. Rowe and Griffith (2015) provide a geologic perspective focused on recognizing seismic fault slip from a range of observables in exhumed fault zones.

Here, I present an overview of geodetic and seismological observations of slow slip, consider results from geophysical imaging of creeping faults, assess geologic studies of faults that may represent exhumed examples of slow slip and its environment, and finally discuss recent laboratory and theoretical studies that try to explain the mechanics and dynamics of slow slip. A glossary of terms (Table 1) and summary of the tools of slow slip research (Table 2) are provided. The emphasis is on providing a balanced and interdisciplinary overview of recent advances in slow slip research and highlighting some outstanding questions for future investigations.

2. The geophysics of slow slip

While the initial discovery of fault creep came from observations of damage to manmade structures straddling faults, the quantification of slow slip in space and time requires geophysical observations. Geodetic measurements of surface deformation along faults allow for mapping out the kinematics of slow slip below the Earth's surface. There are also certain types of seismic signals (e.g., repeating earthquakes, earthquake swarms, and tremors) that help illuminate slow slip at depth. Geophysical imaging (e.g., seismic tomography, receiver functions and electrical resistivity) provides valuable insights into the structure and environment of slow slip deep in the crust, including information about the width, compo-

Table 2
Tools of slow slip research from top to bottom.

	Distribution of slow slip in space and time (from steady creep to SSE)	Fault zone structure, fluids and conditions	Fault zone rheology
Shallow: Upper few km	Onshore: creepmeters, InSAR, near-field GNSS and/or terrestrial surveying, and strainmeters. Limited microseismicity.	Onshore: Shallow geophysical imaging. Geologic field studies, drilling.	Frictional modeling of shallow afterslip, modulated surface creep and anthropogenically induced SSEs.
	Offshore: Seafloor acoustic ranging, near-field ocean bottom pressure, and borehole pore pressure, strain- and tiltmeters. Time-dependent tremor and microseismicity as slow slip proxies.	Offshore: Marine seismic reflection imaging. Seafloor drilling.	Laboratory experiments considering frictional properties of fault zone materials.
Intermediate: Seismogenic depth range	Onshore: Kinematic (time-dependent for SSE) model inversion of GNSS, InSAR etc. Repeating earthquakes and microseismicity in space and time.	Onshore: Probing of seismic velocities, velocity ratios and attenuation. Electrical resistivity. Geologic field studies of exhumed fault zones.	Modeling of afterslip and spontaneous or triggered SSEs as frictional, damage and/or viscous process.
	Offshore: Model inversion of GNSS and seafloor geodetic measurements. Repeating earthquakes and microseismicity as slow slip proxies.	Offshore: Marine seismic reflection, tomography. Deep drilling.	Experiments considering range of fault zone materials, scales, deformation processes, and environmental conditions.
Deep: Below seismogenic zone	Model inversion of GNSS, and/or strainmeter, tiltmeter and InSAR data. Tremor and low-frequency earthquakes as proxies of slow slip in space and time.	Probing of seismic velocities, velocity ratios and attenuation. Electrical resistivity.	Modeling of deep afterslip transients, SSEs and tremor as frictional and/or mixed-mode process.
		Geologic field studies of exhumed fault zones.	Experiments considering deformation processes at high temperature, pressure and fluid pressures.

sition and fluid pressure of creeping faults. I consider examples of slow slip behavior from top to bottom of mostly strike-slip and subduction fault systems (Fig. 1).

2.1. Geodetic observations

The first observations of offset manmade structures by slow slip were made on continental strike-slip faults, including the central creeping segment of the San Andreas Fault (Steinbrugge et al., 1960), the Hayward Fault (Louderback, 1942), and the Ismetpasa segment of the North Anatolian Fault in Turkey (Ambraseys, 1970). Creepmeters directly measure offsets across a fault surface trace, using rods or wires to capture shallow slow slip and creep events at sub-mm accuracy and high temporal resolution (Bilham et al., 2004, and references cited therein). Frequent geodetic surveys of closely spaced measurement points across fault traces with theodolites, Global Navigation Satellite System (GNSS) receivers and other geodetic positioning systems capture shallow fault creep (e.g., Lienkaemper et al., 2014). Borehole strain- and tiltmeters can detect short-term elastic deformation transients from nearby SSEs at or below the earth's surface, which can be modeled to quantify the slip on the fault (e.g., Linde et al., 1996). The high spatial resolution (10s of m), global spatial coverage and precision (sub-cm over short distances) of synthetic aperture radar interferometry (InSAR) (Bürgmann et al., 2000) is particularly well suited to image the distribution of shallow creep on faults around the world (e.g., Doubre and Peltzer, 2007; Jolivet et al., 2012; Thomas et al., 2014a; Chaussard et al., 2015; Turner et al., 2015; Pousse Beltran et al., 2016).

While early fault creep observations were limited to near the Earth's surface, aseismic slip can also occur at all depths within the seismogenic zone of faults and below (Fig. 1). To map out the distribution of fault creep in the subsurface requires precise displacement measurements over a range of distances from a fault and inverse modeling approaches (e.g., Harris and Segall, 1987; Jolivet et al., 2015). Improvements in space geodetic measurements and model inversion schemes have led to improved resolution of the distribution of locked and creeping fault areas on continental strike-slip (e.g., Jolivet et al., 2015, Fig. 2c), thrust (e.g., Thomas et al., 2014a) and normal faults (e.g., Anderlini et al., 2016). Fig. 2 illustrates the wide range of spatial and temporal scales of slow slip at the example of the central San Andreas Fault. Similarly complex slow-slip behavior has been found along many partially coupled continental faults around the world (Harris, 2017). A combination of continuous GNSS measurements, InSAR time series and other geodetic observations provide the spatial and temporal sampling to resolve time dependent variations of fault creep at depth, including SSEs and postseismic afterslip (e.g., Shirzaei and Bürgmann, 2013; Avouac, 2015, and references cited therein; Rousset et al., 2016). Slow fault creep is likely down dip of the seismogenic zone, where high temperatures and pressures allow for continuous aseismic shearing (Savage and Burford, 1970; Blanpied et al., 1991); however, the width and rheological properties of this lower crustal deformation zone are difficult to ascertain (Bürgmann and Dresen, 2008).

The apparent deficit of seismic moment release on many subduction thrusts and oceanic transform faults suggests that slow slip must also be ubiquitous on many of the world's offshore faults (Bird and Kagan, 2004). Creep on these oceanic plate boundary faults is more challenging to measure due to the sometimes-poor resolution of slip models based on terrestrial geodetic observations alone. The first-order distribution of coupling on subduction thrusts can be inverted from land-based GNSS velocities, but usually with little resolution near the trench (e.g., Chlieh et al., 2008; Loveless and Meade, 2011). Seafloor measurement techniques are beneficial to better capture offshore slow slip. Direct-path acoustic ranging, ocean bottom pressure sensors, coupled GNSS – acoustic systems, and pore–pressure measurements in boreholes have all proven capable of observing slow slip on offshore faults (Bürgmann and Chadwell, 2014, and references cited therein; Wallace et al., 2016; Araki et al., 2017).

As the landward edge of the locked portions of many subduction zones roughly coincides with the overlying coastline, details of slow slip behavior in the downdip region of subduction rupture asperities are generally resolvable with terrestrial geodetic observations. The first detections of deep-seated subduction SSEs were made with continuous GNSS measurements in SW Japan and the Cascadia subduction zone (Hirose et al., 1999; Dragert et al., 2001). GNSS, tiltmeter and strainmeter observations clearly document SSEs deep on many of the world's subduction thrusts,

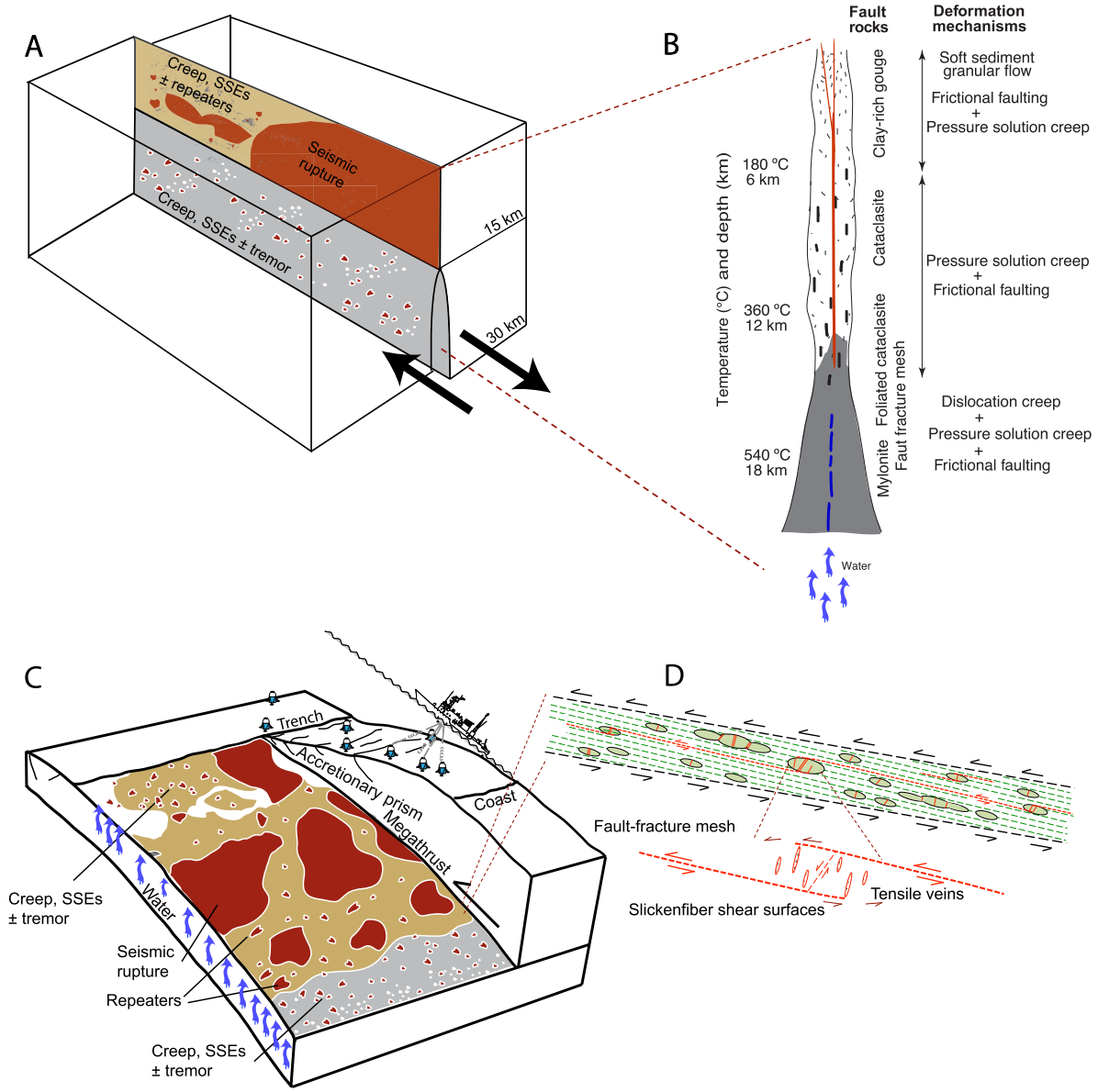

Fig. 1. Fault structure and slip behavior of strike-slip and subduction thrust faults. (a) Schematic illustration of the distribution of seismic and aseismic slip and tremor on the partially coupled San Andreas Fault near Parkfield (modified from original image by Kaj Johnson, written comm., 2017). Fluids at high pressures in the lower crust may be derived from underlying paleo-subduction rocks. (b) Conceptual section across strike-slip fault illustrating depth distribution of fault zone rocks and deformation mechanism accommodating slow slip (based on Fagereng and Toy, 2011). (c) Distribution of seismic and aseismic slip and tremor on partially coupled subduction zone. Fluids at high pressure are derived from compaction of porous fault-zone mélange at shallow depths and metamorphic dehydration reactions in subduction slab deep below (based on Lay et al., 2012). (d) Close-up of fault-zone structure with ductile foliation (green dashed lines), competent lenses (green) with tensile veins (red) and shear-parallel veins (slickenfiber) making up a distributed fault-fracture mesh structure (modified from Sibson, 2017).

finding a wide range of SSE dimensions, slip and duration (e.g., Ohta et al., 2006; Outerbridge et al., 2010; Radiguet et al., 2012; Avouac, 2015, and references cited therein). More enduring slip episodes spaced years apart often occur immediately down-dip of the locked megathrust, while smaller, shorter, and more frequent slip events are located further down dip at 30–40 km depth and are accompanied by abundant tremors (see section 2.2). Nishimura et al. (2013) resolve ~150 of these short-term SSEs from continuous GNSS time series in SW Japan. Not all subduction zones show such active slow-slip behavior. While the Sumatra megathrust features creeping sections that are anti-correlated with the rupture zones of historic earthquakes (Chlieh et al., 2008) and accelerate during afterslip episodes (Hsu et al., 2006), a careful analysis of data from coastal continuous GNSS stations failed to find a single spontaneous slow slip transient during a 10-yr period (Feng et al., 2015). However, Tsang et al. (2015) found evidence in coral microatoll growth records for a 1966–1981 deformation transient that they attribute to an enduring SSE on the Sumatra megathrust.

Yokota et al. (2016) relied on seafloor GNSS-acoustic measurements to better detect offshore areas of low coupling on the Nankai subduction zone. The slow slip zones appear to bound and complement areas of peak slip in large historic earthquakes, including a zone of creep near the trench, up dip of the 1944 M 8.1 Tonankai rupture zone (Fig. 3a). Araki et al. (2017) used observations of seafloor borehole pressure to document SSEs in this shallow zone, often accompanied by clusters of low-frequency earthquakes. These near-trench slip transients recur every 8 to 15 months and accommodate roughly half of the total plate convergence rate. Two of these SSEs were dynamically triggered by the 2011 Tohoku-oki and 2016 Kumamoto earthquakes, suggesting the shallow megathrust is mechanically weak (Araki et al., 2017). In 2014, Wallace et al. (2016) captured a large shallow SSE on the

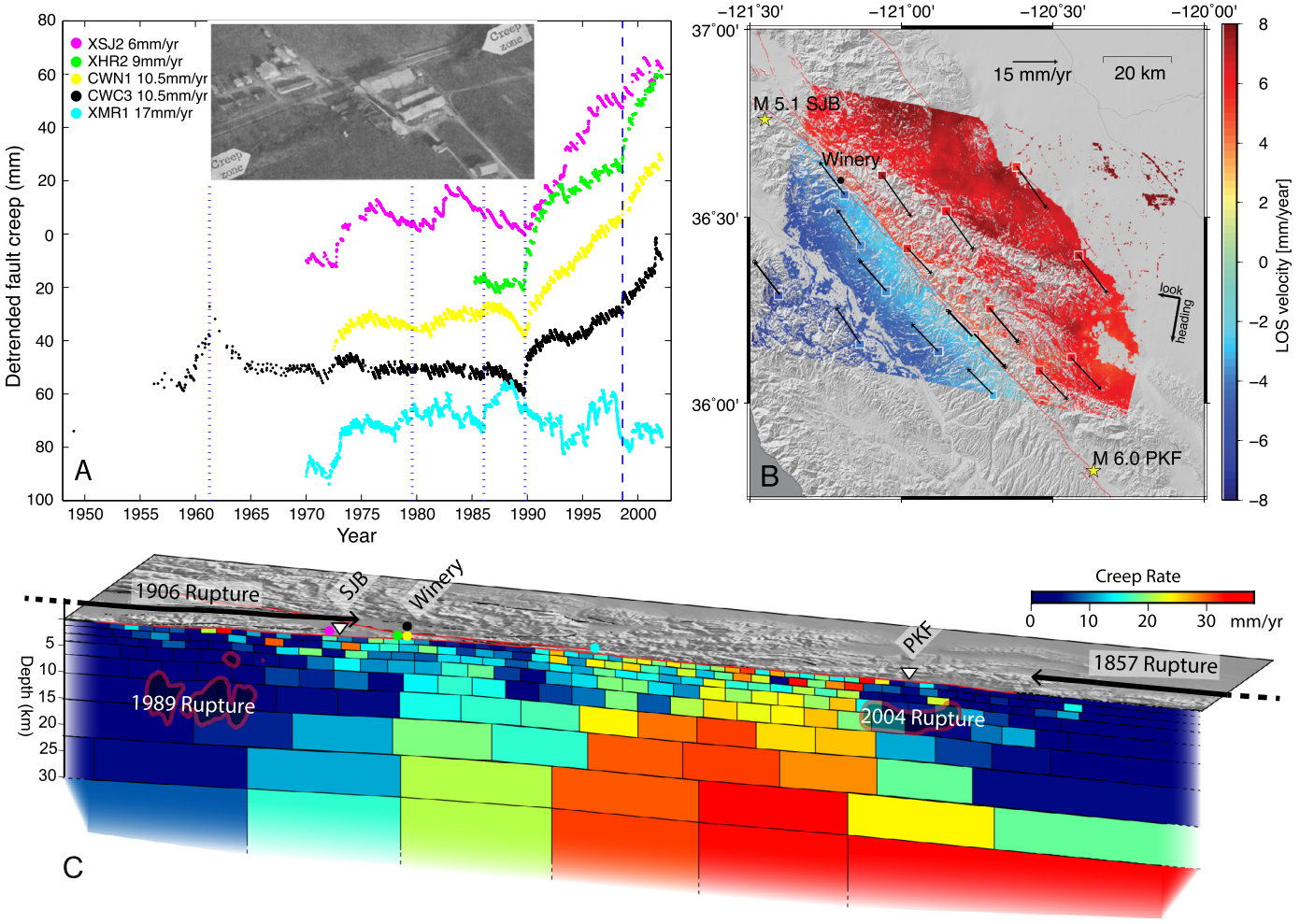

Fig. 2. Geodetic observations of slow slip on the central creeping segment of the strike-slip San Andreas Fault. (a) Surface creepmeter records from instruments installed at the Taylor Winery (CWC3, CWN1) and nearby sites (see (c) for locations). The slip time series are detrended by the rates noted in the legend (modified from Bokelmann and Kovach, 2003). Inset image shows aerial view of place of first published creep evidence from fault-crossing structures at the winery (Steinbrugge et al., 1960). (b) 2006–2010 InSAR and GNSS measurements along the creeping segment (modified from Turner et al., 2015). (c) 3D view of kinematic model of slow-slip-rate distribution on the fault inverted from InSAR and GNSS measurements between San Juan Bautista (SJB) and Parkfield (PKF) (modified from Jolivet et al., 2015). Colored circles show locations of correspondingly colored creepmeters whose records are shown in (a). Grey-shaded areas outline rupture contours of the 1989 M 6.9 Loma Prieta and 2004 M 6.0 Parkfield earthquakes. Arrows show the approximate extent of the 1906 M 7.9 San Francisco and 1857 M 7.9 Fort Tejon earthquake ruptures.

Hikurangi subduction thrust in New Zealand using a temporary array of ocean bottom pressure sensors and permanent land-based GNSS stations (Fig. 3b). This slip patch was reactivated as part of a much larger, but less enduring slow slip episode that was dynamically triggered by the 2016 M 7.8 Kaikoura earthquake and propagated along a ~300-km-long section of the shallow plate interface (Wallace et al., 2017, Fig. 3c).

2.2. Seismologic constraints

Even though slow slip is generally considered to be aseismic by definition, seismological observations of low-frequency seismic waves and the analysis of secondary seismic events provide valuable constraints on its occurrence. Some SSEs slip at rates that are fast enough that they emit some long-period seismic energy, which requires broadband seismometers to be detected (Beroza and Jordan, 1990). Such slow earthquakes, strongly or fully depleted in high-frequency energy, are mostly found along oceanic transform faults and subduction zones (Beroza and Jordan, 1990, and references cited therein). Very-low-frequency earthquakes are relatively small ($M_w = 3$–4) slow earthquakes (Ito et al., 2007; Beroza and Ide, 2011) that are found both in the very shallow (upper 5 km) and deep (30–40 km) portions of some subduction zones, generally in association with tectonic tremor (see below).

There are seismic signals that can reveal the existence and provide additional information about the spatiotemporal distribution of slow slip at depth. Repeating earthquakes have nearly identical seismic waveforms, indicating these events have effectively the same hypocenters and mechanisms. Such repeaters are understood to result from recurring rupture of small asperities that are driven to failure by creep on the surrounding fault (e.g., Nadeau and McEvilly, 1999). The larger the repeating earthquakes in a sequence, the greater the increment of slip they record as they catch up with the creeping fault. Thus, the magnitude and recurrence intervals of repeating earthquakes can be used to estimate the slow slip driving their failures. The quantification of slow slip using repeaters often relies on a geodetically calibrated magnitude-to-slip relation established for the San Andreas fault (Nadeau and Johnson, 1998). Slip estimates can also be deduced from relationships assuming constant rupture area or stress drop (Rubinstein et al., 2012) or from frictional fault models (Beeler et al., 2001; Mavrommatis et al., 2015). Not all creeping faults feature repeaters, and the absence of such events does not imply there is no slow slip.

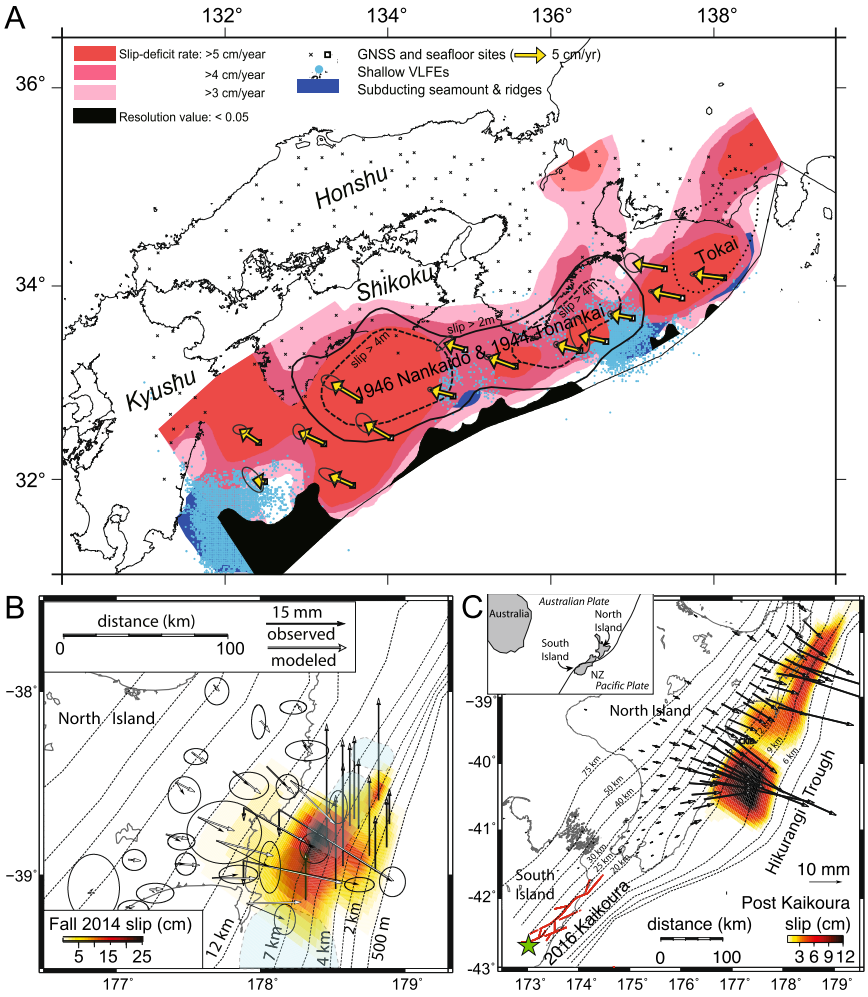

Fig. 3. Slow slip on subduction megathrusts from terrestrial and seafloor geodesy. (a) Interseismic coupling on the Nankai subduction zone in southwest Japan obtained from inversion of land-based GNSS (crosses) and seafloor GNSS-acoustic (squares with yellow arrows showing velocities with respect to Amurian plate). Very-low-frequency earthquakes (blue dots) and subducted seamounts and ridges (blue polygons) correlate with areas of inferred slow slip. Rupture zones of historic megathrust earthquakes correlate with areas of high coupling (modified from Yokota et al., 2016). (b) Spontaneous slow slip event near the trench on the Hikurangi megathrust captured by land-based GNSS and offshore seafloor pressure sensors (modified from Wallace et al., 2016). Zones of high-amplitude interface seismic reflectivity (dashed outlines) have been correlated with locations of previous SSEs and may highlight fluid-rich sediments that have been entrained down dip of subducting seamounts (Bell et al., 2010). (c) Unprecedented slow-slip episode involving most of the shallow Hikurangi megathrust triggered by the 2016 M 7.8 Kaikoura earthquake (green star and red rupture surface trace). The SSE followed strong dynamic stressing in the shallow accretionary wedge acting as a waveguide for the mainshock surface waves (modified from Wallace et al., 2017). Dashed lines show depth to the active plate interface.

Repeating earthquakes recur at quasi-regular intervals on creeping sections of transform (e.g., Peng and Ben-Zion, 2005; Turner et al., 2015; Dominguez et al., 2016; Hayward and Bostock, 2017; Materna et al., 2018), extensional (e.g., Valoroso et al., 2017; Vuan et al., 2017), and convergent (e.g., Chen et al., 2007; Uchida and Matsuzawa, 2013; Meng et al., 2015; Dominguez et al., 2016; Yao et al., 2017) plate boundary faults from around the world. Recurrence intervals are shortened during accelerated creep associated with postseismic afterslip and slow slip transients (e.g., Uchida and Matsuzawa, 2013; Turner et al., 2015; Uchida et al., 2016) (Figs. 4a and 5a). Accelerated repeater occurrences suggesting precursory slow slip also accompanied the foreshock sequences of the 2011 M_w 9.0 Tohoku-oki and 2014 M_w 8.2 Iquique, Chile earthquakes (Kato et al., 2012; Meng et al., 2015). Both along the central creeping segment of the San Andreas fault (Turner et al., 2015, Fig. 4a) and on the subduction thrust of northeast Japan (Uchida et al., 2016), repeating earthquakes reveal episodic slip-rate accelerations every few years, sometimes correlated with larger nearby earthquakes on the respective plate-boundary fault.

A subset of earthquake swarms (seismicity bursts that do not exhibit clear mainshock–aftershock patterns) appear to be the result of SSEs on partially coupled faults (Vidale and Shearer, 2006; Lohman and McGuire, 2007). As other processes, such as fluid diffusion, can also produce seismic swarms, their association with slow slip is often non-unique. A more rapid and near-linear propagation rate (0.1–1 km/h) of swarm events may be an indicator of slow slip driving an episode (Roland and McGuire, 2009). Some foreshock sequences of large earthquakes are swarms, especially on oceanic transforms (Roland and McGuire, 2009) and subduction thrusts (Nishikawa and Ide, 2017, and references cited therein), suggesting that they illuminate SSEs that sometimes culminate in a larger seismic rupture (Brodsky and Lay, 2014).

The discovery of tectonic tremor down dip of the seismogenic zone of the Nankai subduction thrust in southwest Japan (Obara, 2002) opened a new chapter in the study of aseismic fault slip. To date, tremor activity has been found on at least a dozen plate boundary fault zones around the world (Obara and Kato, 2016, and original references cited therein). The tremor signal consists of enduring emissions (up to hours at a time) of low-frequency seismic energy and appears to be made up of a large numbers of short low-frequency earthquakes (<1 s duration) (Shelly et al., 2006; Shelly, 2017b). Tremor is sometimes accom-

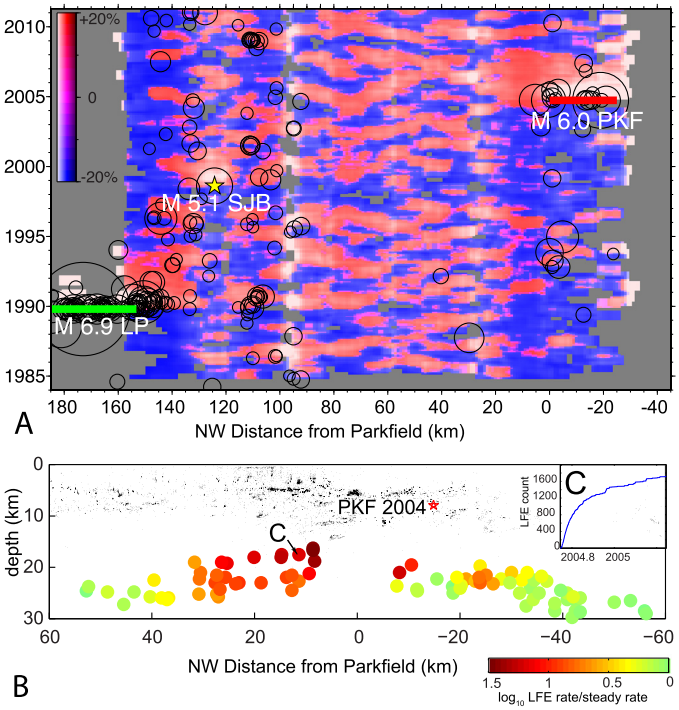

Fig. 4. Time-dependent slow slip from repeating earthquakes and LFEs on the central San Andreas Fault. (a) Subsurface slow-slip-rate changes inferred from repeating-earthquake recurrence intervals as a function of distance along the fault and time from 1984 to 2010 (modified from Turner et al., 2015). Red and blue areas indicate slip rates that are ≥20% higher or lower than the long-term average at that location, white shading indicates increased uncertainties. The creeping section appears to accelerate in relatively regular pulses every ~2 years. Postseismic accelerations from 1989 Loma Prieta (LP), 1998 San Juan Bautista (SJB) and 2004 Parkfield (PKF) mainshocks endured for several years (see Fig. 2 for event locations). M ≥ 3 earthquakes are shown as black circles. (b) Lower-crustal afterslip of 2004 M_w 6.0 Parkfield earthquake revealed by the ratio of the average rate of co-located low-frequency-earthquakes during the first 30 days and their average rate during the previous 6 months. The inset (c) shows cumulative number of events in the family of low-frequency earthquakes labeled C. The red star shows the hypocenter of the 2004 mainshock. The long-term fault slip rate is ~34 mm/yr.

panied by much longer (10–200 s duration) very-low-frequency earthquakes (Beroza and Ide, 2011). Where independent geodetic data exist, it can be shown that tremors are the direct product of slow slip (e.g., Rogers and Dragert, 2003; Bartlow et al., 2011; Nishimura et al., 2013); however, deep-seated slow slip may occur at times and in places without accompanying tremor (e.g., Wech and Bartlow, 2014, Fig. 5c). Tremor and/or slow slip episodes in the deep roots of the southwest Japan, Alaska, Cascadia, Costa Rica, Mexico, and New Zealand subduction zones recur at intervals of months to several years (Obara and Kato, 2016, and original references cited therein), but tremor appears to occur nearly continuously along the eastern end of the Alaska-Aleutian subduction zone (Wech, 2016). Tremors and very-low-frequency earthquakes are also found in some poorly-coupled shallow sections of subduction zones in Japan, New Zealand and Costa Rica, while in other areas shallow SSEs are accompanied by bursts of microseismicity (Saffer and Wallace, 2015, and original references cited therein).

Along the 140-km-long section of the central San Andreas fault around Parkfield, tectonic tremor and low-frequency earthquakes illuminate slow-slip behavior on the lower crustal portions of the fault (Guilhem and Nadeau, 2012; Shelly, 2017b; Thomas et al., 2018). Template-matching analysis of more than a million low-frequency earthquakes resolved the location of 88 well-located families hosting these events. This large number of events allows for detailed analysis of the modulation of slow slip by static stress changes from Earth tides (Thomas et al., 2012) and nearby earthquake ruptures (Johnson et al., 2013, Fig. 4b), and reveals frequent dynamic triggering by teleseismic and regional earthquakes (Shelly, 2017b, and references cited therein).

2.3. The environment of slow slip from geophysical imaging

To understand why faults creep where they do, it is important to understand the structure, make-up and physical environment of slowly slipping fault segments. This motivates geophysical imaging of faults at depth and geological studies of exhumed fault zones (see Section 3). Seismic imaging methods provide information about seismic wave speeds, and thus elastic properties affected by differences in composition, crack density and fluids in and near a fault zone. Electric resistivity measurements can provide complementary information about the distribution of conductive fluids. Repeated observations of fault-zone properties allow for studying any temporal variations associated with slow slip episodes, possibly related to fracturing and fluid flow. It has not been easy to find a unique geophysical signature of slow slip, with the focus of such studies being on observations that reflect the presence and high pressure of fluids near the fault, as well as the thickness of the imaged fault zone. I summarize results from a few strike-slip and subduction zones below, well aware that there have been many equally intriguing findings in other areas.

Along the creeping San Andreas fault near Ciniega Winery (Fig. 1), seismic tomography (Thurber et al., 1997), fault zone trapped waves (Li et al., 1997) and a combination of head waves and direct P waves (Lewis et al., 2007) have been used to image a shallow low-velocity fault zone. The trapped S-waves suggest a ~120-m thick shallow fault zone, while the seismic tomography results show a ~1-km-wide zone of high P-wave to S-wave velocity ratio down to ~6 km. Bedrosian et al. (2004) use high-resolution magnetotelluric imaging to document a zone of high conductivity and inferred fluid content alongside this section of the fault, which may help provide conditions for aseismic slip to mid-crustal depth. Comparable results have been obtained along the southernmost section of the creeping section of the San Andreas fault near Parkfield, but also point to the likely complexity and heterogeneity of the fault zone (e.g., Lewis and Ben-Zion, 2010; Becken et al., 2011; Zeng et al., 2016). The seismic velocity and electrical resistivity structure across the >15-km-deep San Andreas fault below the seismogenic zone at Parkfield (Fig. 6) also suggests a low-velocity zone and involvement of fluids (Becken et al., 2011; Zeng et al., 2016). Fluids at high pressure may help explain the occurrence of slow-slip transients, evidenced by tectonic tremor and low frequency earthquakes, along the lower-crustal San Andreas fault in this area (Shelly, 2017a).

Particularly interesting imaging results of creeping versus earthquake-producing fault segments come from oceanic transform faults. Using active source refraction seismology, Roland et al. (2012) document a strong, >2-km-wide low-velocity zone (Fig. 7b) along the central section of the Gofar transform fault on the East Pacific Rise (Fig. 7a), which they attribute to fluid-filled fractures. This high-porosity section of the fault features abundant micro-seismicity and is inferred to be a zone of slow slip bounding seismic rupture asperities that lack a well expressed low-velocity zone. McGuire et al. (2012) provide evidence of changing fault-zone properties during a foreshock swarm and apparent slow slip episode in the low-velocity zone adjacent to and preceding a M_w 6 mainshock of the Gofar transform (Fig. 7c). The foreshock activity resulted in a ~3% reduction in seismic shear-wave speeds, likely due to enhanced fluid circulation in the 10-km-long swarm zone (McGuire et al., 2012; Froment et al., 2014). These results suggest a strong contrast between a highly damaged and fluid-filled low-velocity fault zone

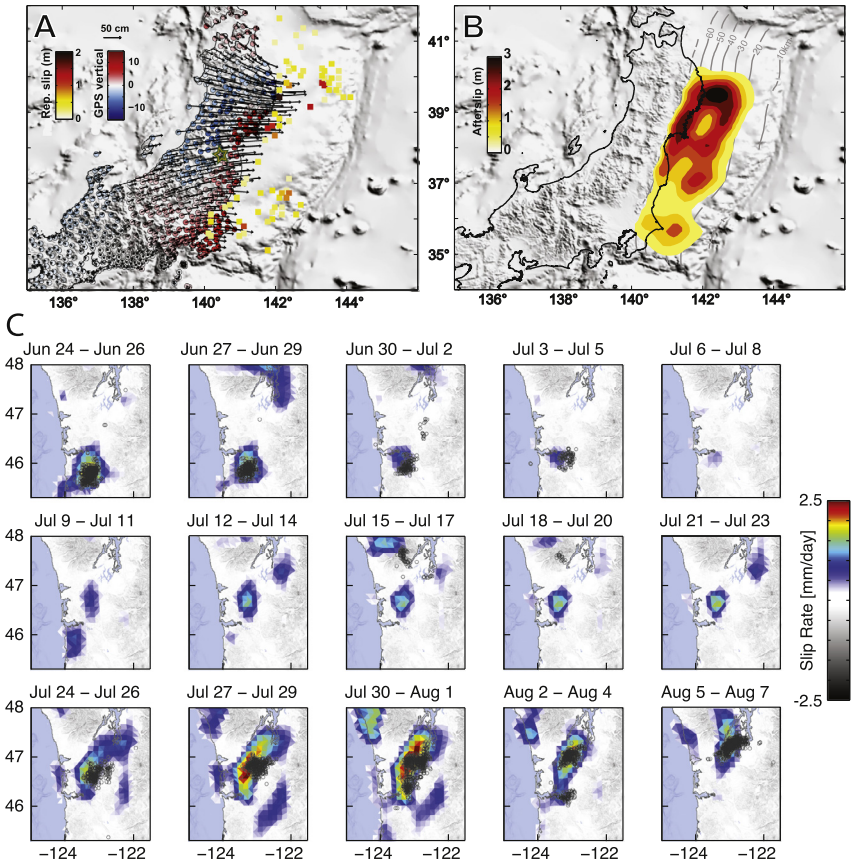

Fig. 5. Time-dependent slow slip on subduction thrusts inferred from repeating earthquakes, tremors and GNSS data. (a) Afterslip after the M_w 9.0 Tohoku-oki megathrust earthquake from repeating earthquakes shown with onshore GNSS displacements, from 3 days after the March 11 mainshock through June 23, 2012. Each square offshore shows the location of a repeating earthquake sequence and is color-coded by the estimated cumulative postseismic creep (modified from Uchida and Matsuzawa, 2013; Shirzaei et al., 2014). (b) Afterslip model inverted from the GNSS and repeating earthquake data taking into consideration the substantial contribution of viscoelastic relaxation (Hu et al., 2016) to the surface deformation (modified from Shirzaei et al., 2014). (c) Three-day snapshots of tremor locations (black circles) and slow slip rate (color scale in mm/day) inverted from GNSS- and strainmeter time series during an SSE on the Cascadia subduction thrust, in the summer of 2011. During mid-July (middle row), slow slip continued without producing resolvable tremor activity (modified from Wech and Bartlow, 2014).

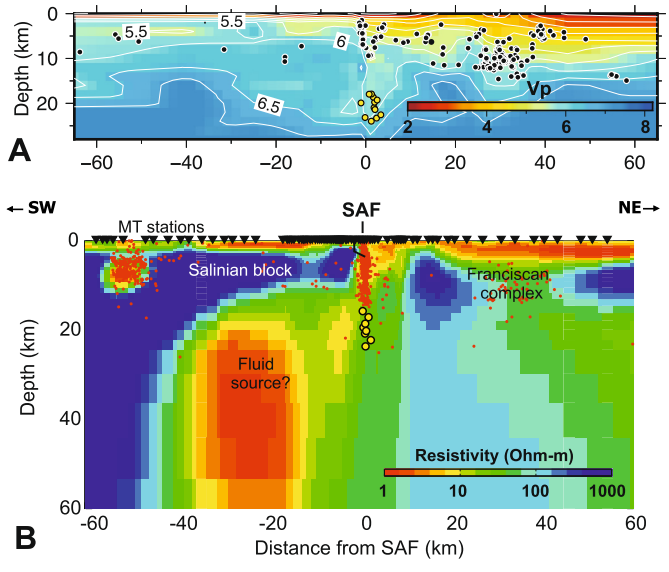

Fig. 6. Profiles of (A) seismic P-wave velocity (modified from Zeng et al., 2016) and (B) electrical resistivity across the San Andreas fault (SAF) near Parkfield (modified from Becken et al., 2011). Black and red dots indicate microseismicity near the lines of section. Yellow circles are low-frequency earthquakes in the lower crust. The base of the crust is at ~30 km depth.

hosting abundant micro-seismicity and episodic aseismic slip and a high-velocity zone hosting large earthquake ruptures.

Geodetic and seismic observations have revealed that many subduction zone thrusts experience (often time-dependent) slow slip, ranging in depth from deep below the seismogenic zone to the trench (see sections 2.1 and 2.2). Geophysical imaging studies have been aimed at finding correlative changes in fault zone properties. Teleseismic receiver functions show that seismic velocities are greatly reduced and P-wave to S-wave velocity ratios are highly elevated in deep subduction thrusts around the world that host tremor and slow slip, suggesting a zone of high porosity and fluid pressure (Audet and Kim, 2016 and references cited there). Audet and Bürgmann (2014) find that the recurrence intervals of SSEs in the tremor zone of global subduction zones linearly decrease with the seismic velocity ratios of the overlying forearc crust, suggesting that SSE behavior is controlled by temperature-dependent silica deposition, permeability reduction and fluid overpressure. At the Cascadia margin, the zone of low seismic velocities and inferred fluid overpressure widens with depth and does not appear to extend into the updip locked zone of the megathrust (Audet and Schaeffer, 2018). From active source seismology, Nedimovic et al. (2003) find that the deep-seated creeping portion of the Cascadia megathrust exhibits a wide zone of strong reflections (>4 km wide), while the shallower locked section features a much narrower (<2 km) reflection. The wider zone of low velocities and reflections at depth hosting episodic slow slip may reflect a vol-

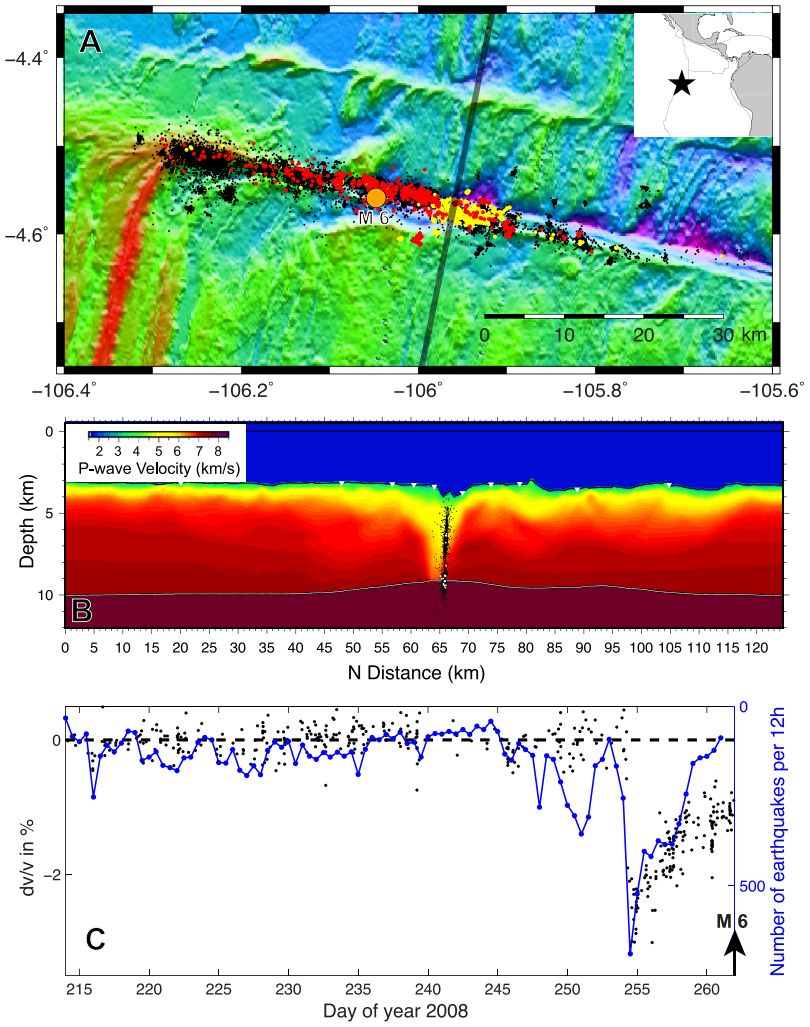

Fig. 7. Seismic swarm activity and slow slip, velocity structure and time-dependent seismic velocity along the Gofar transform fault. (a) Seismicity before and after the 18 September 2008 M_w 6.0 earthquake (orange circle). Foreshocks on 10–12 September (yellow dots) and aftershocks on 18–20 September (red dots) delineate the extent of an inferred precursory SSE and the mainshock rupture, respectively (modified from McGuire et al., 2012). The refraction profile (bold line) crosses through the foreshock zone. (b) Seismic P-wave velocity model (modified from Roland et al., 2012) showing low-velocity zone to the base of the crust. Black dots in (a) and (b) are background seismicity. (c) Measurements of precursory change in seismic P-wave velocity (dv/v) (black dots) during 439 events in the inferred slow-slip zone before the mainshock (day 262). The blue curve shows earthquake rate (events per 12 h) in the larger area (modified from McGuire et al., 2012).

ume of interlayered rock units and ductily sheared and/or fluid saturated fault zone material.

Fluid-rich subducted sediments and high fluid pressure have also been inferred from seismic reflection imaging of shallower slow slip zones of subduction thrusts in Japan (e.g., Kodaira et al., 2004; Tobin and Saffer, 2009) and New Zealand (Bell et al., 2010, Fig. 3b). In contrast, seismic velocities appear to be high, and seismic P-to-S velocity ratios low, in well coupled portions of subduction thrusts hosting great megathrust earthquakes (Zhao et al., 2011; Audet and Schaeffer, 2018). However, at intermediate depths of the subduction plate interface offshore Nicoya, Costa Rica, Audet and Schwartz (2013) find high P-to-S velocity ratios along both coupled and creeping sections.

Further evidence for fluid-filled porosity in areas of slow subduction slip comes from complementary magnetotelluric imaging. High electric conductivity is found in the deep-seated tremor zone of the Cascadia subduction zone where the onset of eclogitization of the downgoing oceanic crust is expected to contribute abundant fluids (Wannamaker et al., 2014). High-resistivity is found in the fully-coupled updip section of the megathrust that also lacks a well-developed low-seismic-velocity zone (Audet and Schaeffer, 2018). Heise et al. (2017) document the electrical resistivity structure of a 12-to-15-km deep portion of the partially coupled Hikurangi subduction interface. They find that a zone of high resistivity corresponds to a locked patch on the plate interface inferred from geodesy, while areas of high conductivity match the location of weak coupling and SSEs. Some of the areas of high conductivity coincide with zones of slow wave speed, high P-wave to S-wave velocity ratios and seismic attenuation on the plate interface (Bassett et al., 2014; Eberhart-Phillips and Bannister, 2015), supporting the view that these are zones of high fluid content and overpressure (Saffer, 2017).

The geophysical imaging studies described above lend support to the idea that fluids and/or fluid-saturated sediments on faults enable (often episodic) aseismic fault slip and suppress the nucleation of earthquake ruptures. The observations allow for fault zone composition and structure (e.g., a sheared mélange of unconsolidated ocean sediments or serpentinite-rich material) to play a role in producing conditions for slow slip at depth. Details of the subsurface geometry, physical properties and environment of fault zones at depth are generally difficult to resolve and there continues to be a need for improved methodologies and rigorous integration of complementary constraints from multiple observation types.

3. The geology of slow slip

Inspired by the geophysical observations of fault creep and its environment in different settings (Section 2), geologists have set out to evaluate exhumed fault zones for diagnostic evidence of slow slip and its causes (e.g., Sibson, 1977). What are the geologic signatures of fault creep, slow slip events and tectonic tremor? What materials, environmental conditions, mineral deformation mechanisms, and structures should we expect to find in such outcrops? How do these slow slip features differ from faults slipping seismically?

One might argue that the lack of evidence of seismic slip is diagnostic of fault creep, or, as Fagereng and Toy (2011) put it, assume that faults are "aseismic until proven guilty of seismic slip". There are few unambiguous indicators of slip at seismic speeds, but solid evidence includes frictional rock melt and mineral-reaction products that indicate high peak temperatures in the fault zone from earthquake slip (Sibson, 1989; Fagereng and Toy, 2011; Rowe and Griffith, 2015). Other proposed diagnostics of dynamic slip include microscopic fabrics indicating fluidized granular flow in fault-zone rocks, polished fault-surface morphologies, and the geometry and distribution of secondary brittle structures that can be related to dynamic stress fields of a propagating earthquake rupture (Rowe and Griffith, 2015 and references cited therein). However, as slow slip can be closely associated with seismic slip in space and time, observations of such high slip-speed indicators do not necessarily rule out an important role of slow slip in an outcrop.

Thus, just as it has been challenging to find geologic diagnostics documenting dynamic earthquake slip, it is difficult to confidently document slow slip speeds in field outcrops. Nonetheless, a number of recent studies have put forward examples of exhumed fault zones from various tectonic settings that exhibit features that can be related to slow slip and/or the generation of tremor. Slow slip has been inferred based on the dominance of fault zone materials that are known to be increasing their frictional strength with increasing slip velocity, observations of ductile shear fabrics due to dislocation and/or pressure-solution creep, and evidence of near-lithostatic fluid pressure from abundant veins in an outcrop. As many creeping faults also produce abundant microseismicity or tremor at depth, geologic studies have also focused on exhumed faults that exhibit evidence of both slow and dynamic fault slip. Given that slow slip occurs over a very wide range of depths and temperatures (Fig. 1), I discuss the geology of slow slip from top to bottom, drawing on examples from strike-slip and subduction settings.

3.1. The geology of shallow creeping faults

Faults that currently creep near the Earth's surface provide direct access to geologists. Cashman et al. (2007) compare near-surface fault-zone structures in unconsolidated sediments above creeping and seismic sections of the San Andreas Fault and find contrasting degrees of cataclasis, porosity and fabric development that may be diagnostic of seismic and aseismic slip. The SAFOD was drilled through two actively creeping fault strands at ∼2.7 km depth and 110–115 °C (Zoback et al., 2010; Lockner et al., 2011). Well-casing deformation documents the locations of active slow slip, coincident with foliated gouge zones consisting of metasomatic reaction products of serpentinite and quartzofeldspathic host rock, dominantly the smectite clay mineral saponite (Fig. 8a). Samples from the ∼2-m-wide gouge zones (Fig. 8a) are frictionally weak ($\mu \approx 0.15$) and strongly velocity strengthening in character, whereas rocks from the surrounding ∼200-m-wide damage zone are modestly velocity strengthening but have higher friction values ($\mu \approx 0.5$) (Carpenter et al., 2011; Lockner et al., 2011). Fluid pressures in the fault zone are not elevated. As saponite is unstable at >150 °C, other mineral phases such as talc, which is stable throughout the seismogenic zone (Moore and Rymer, 2007), or high fluid pressure may be responsible for creep inferred at greater depths on the San Andreas fault. Microstructural investigations of SAFOD samples and experimental results suggest that pressure solution creep (fluid-assisted diffusive mass transfer) may also play an important role in accommodating both shallow and deeper aseismic slip (e.g., Richard et al., 2014). Serpentinite entrained in the fault zone has also been observed in outcrops along the creeping section of the San Andreas (Moore and Rymer, 2007) and here mineralogic composition may be the primary cause of shallow fault creep.

Along creeping sections of the reverse Longitudinal Valley Fault in Taiwan (e.g., Thomas et al., 2014b, Fig. 8b), and the strike-slip North Anatolian Fault in Turkey (e.g., Kaduri et al., 2017, Fig. 8c), there are fault outcrops of heterogeneous mixtures of clays and other velocity-strengthening and low-friction minerals, suggesting lithological control of shallow fault behavior. Both of these studies infer that, in addition to frictional sliding, pressure-solution creep is an important deformation mechanism contributing to the development of foliated gouge fabrics and localization of aseismic slip.

Field investigations of exhumed subduction thrusts, raised from a few km deep and temperatures <250 °C, constrain the environment and mechanical processes of shallow slip on megathrusts (Saffer and Wallace, 2015, and references cited therein). Examples include the exhumed Shimanto accretionary prism in SW Japan (Saito et al., 2013) and the Franciscan subduction complex in California (Meneghini and Moore, 2007). The shallow fault zones contain sedimentary clay minerals and quartz and feature abundant veining that intensifies with depth. Free water in the subducted crust and dehydration of opal and clay minerals provide sources of water. Deformation of such subduction mélange shear zones tends to be distributed across multiple fault strands and involves heterogeneous lithologies and fluids at high pressure. Experiments on geologic samples (Saito et al., 2013) and materials from scientific drilling of active near-trench thrusts (Ikari et al., 2013; Ikari and Kopf, 2017) allow for both velocity-strengthening and unstable slip (see Section 4.2), consistent with geodetic and seismologic evidence of low frictional strength and variable slip behavior of shallow subduction thrusts (see Section 2).

3.2. The geology of slow slip at seismogenic depths

Geophysical evidence (see section 2) documents aseismic fault slip at all depths, including the seismogenic zone that contains most small and large earthquakes and generally coincides with the depth extent of large earthquake ruptures (e.g., Sibson, 1982). Fagereng and colleagues (Fagereng et al., 2010; Fagereng and den Hartog, 2017, and related references cited therein) examined macro- and microstructures in an exhumed megathrust in the Chrystalls Beach Complex, New Zealand to argue that pressure solution creep in concert with frictional sliding (Fig. 9a) allows for the dominantly aseismic accommodation of megathrust slip at temperatures of 250–300 °C. The geometry of associated tensile and shear veins organized in a fault–fracture mesh (Figs. 1d and 9b) suggests that episodic slip occurred in a fluid-overpressured, heterogeneous shear zone, possibly reflecting the occurrence of associated small earthquakes or tremor (Fagereng et al., 2010; Fagereng and Harris, 2014). Rowe et al. (2011) describe another plate-boundary subduction thrust exposed at Pasagshak Point, Kodiak Island, which features evidence for seismic deformation (including frictional rock melt), rapid aseismic slip episodes suggested by non-foliated cataclasites (Fig. 9c), and slow fault creep indicated by well-organized cataclastic shear foliations (Fig. 9d), with pressure solution and granular flow accommodating slow slip at

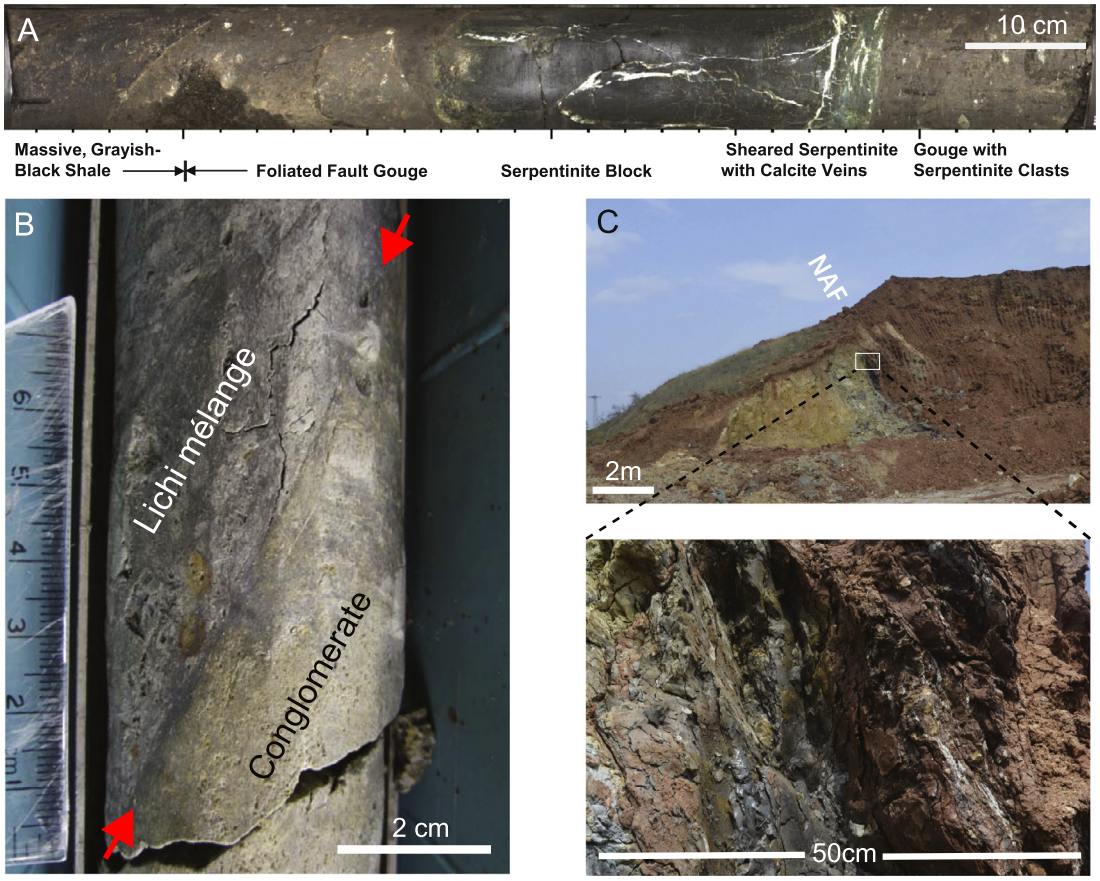

Fig. 8. Geologic examples of faults experiencing active shallow creep. (a) Core sample from the San Andreas fault from SAFOD borehole at ~2.7 km depth, 110–115 °C and moderate fluid pressure (original image from M. Zoback, written comm., 2017). The actively creeping gouge zone, dominantly composed of saponite, is frictionally weak and velocity strengthening (Lockner et al., 2011). (b) Core sample from Longitudinal Valley thrust fault at ~50 m depth, juxtaposing the Lichi mélange with footwall conglomerates (from Thomas et al., 2014a, 2014b original image provided by M. Thomas, written comm., 2018). (c) Field exposure of creeping North Anatolian Fault segment near Ismetpasa (from Kaduri et al., 2017, original image provided by F. Renard, written comm., 2018). The gouge zone shown in the close-up has substantially higher concentrations of quartz and insoluble smectite and other sheet silicates than the volcanic host rocks.

ambient temperatures of about 250 °C. While the unique association of geologic features with rapid and slow slip remains challenging, these observations seem consistent with the behavior inferred for partially coupled fault zones from geophysical observations.

3.3. Geological evidence of slow slip near the brittle-ductile transition

Near the base of the seismogenic zone, rising temperatures and pressures allow for an increasing role of ductile deformation processes in some minerals, providing conditions for aseismic shear and a transition to increasingly viscous deformation (e.g., Handy et al., 2007). Angiboust et al. (2015) examine the remnants of a paleo-subduction thrust in the Swiss Alps exhumed from 30–40 km depth and 400–500 °C paleo-temperatures (Fig. 10). They document mylonitic shear zones, tens-of-meters thick cataclastic fault strands, and abundant tensile veins, all of which appear to be mutually overprinted. The inferred several-orders-of-magnitude fluctuations of deformation rates may reflect the occurrence of slow slip at highly variable speed, as well as the occurrence of dynamic slip, possibly in the form of tremor. The pervasive veining is indicative of high fluid pressures. Similarly heterogeneous materials and deformation styles, as well as abundant veining are found in other fault zones exhumed from comparable depths, such as the Beagle Channel thrust shear zones in southern Chile (Hayman and Lavier, 2014) and the exhumed Damara accretionary prism in Namibia (Fagereng et al., 2014).

Behr et al. (2018) examined an exhumed subduction complex in outcrops on Syros Island, Greece, which they argue to be a representative candidate for a slow-slip and tremor producing fault zone. Faulting occurred near the transition from blueschist to eclogite metamorphic assemblages, at 450–550 °C. Here, blueschist-grade rocks exhibit distributed viscous deformation by dislocation creep, whereas eclogite blocks in the blueschist matrix deform by brittle shear fracture and tensile veining. Thus, the coexistence of aseismic and seismic failure indicated for deep-seated tremor-source regions may be a reflection of variable metamorphic grade, rather than heterogeneous composition.

In the wide brittle–ductile transition regime, heterogeneous composition, metamorphic grade and fluid pressure conditions may allow seismic and aseismic frictional slip, tensile fracturing, pressure-solution creep, and dislocation creep to coexist to produce deformation that may be highly variable in space and in time and allows for the generation of SSEs and tremor.

4. The mechanics of slow slip

4.1. Slow slip in computational models

The most commonly used framework to model the mechanics of slow slip is rate-and-state friction (Dieterich, 1979). These empirically derived friction equations are based on laboratory experiments that show that the shear stress supported by a frictional surface is well described as a logarithmic function of the fault slip rate and one or more state variables characterizing the

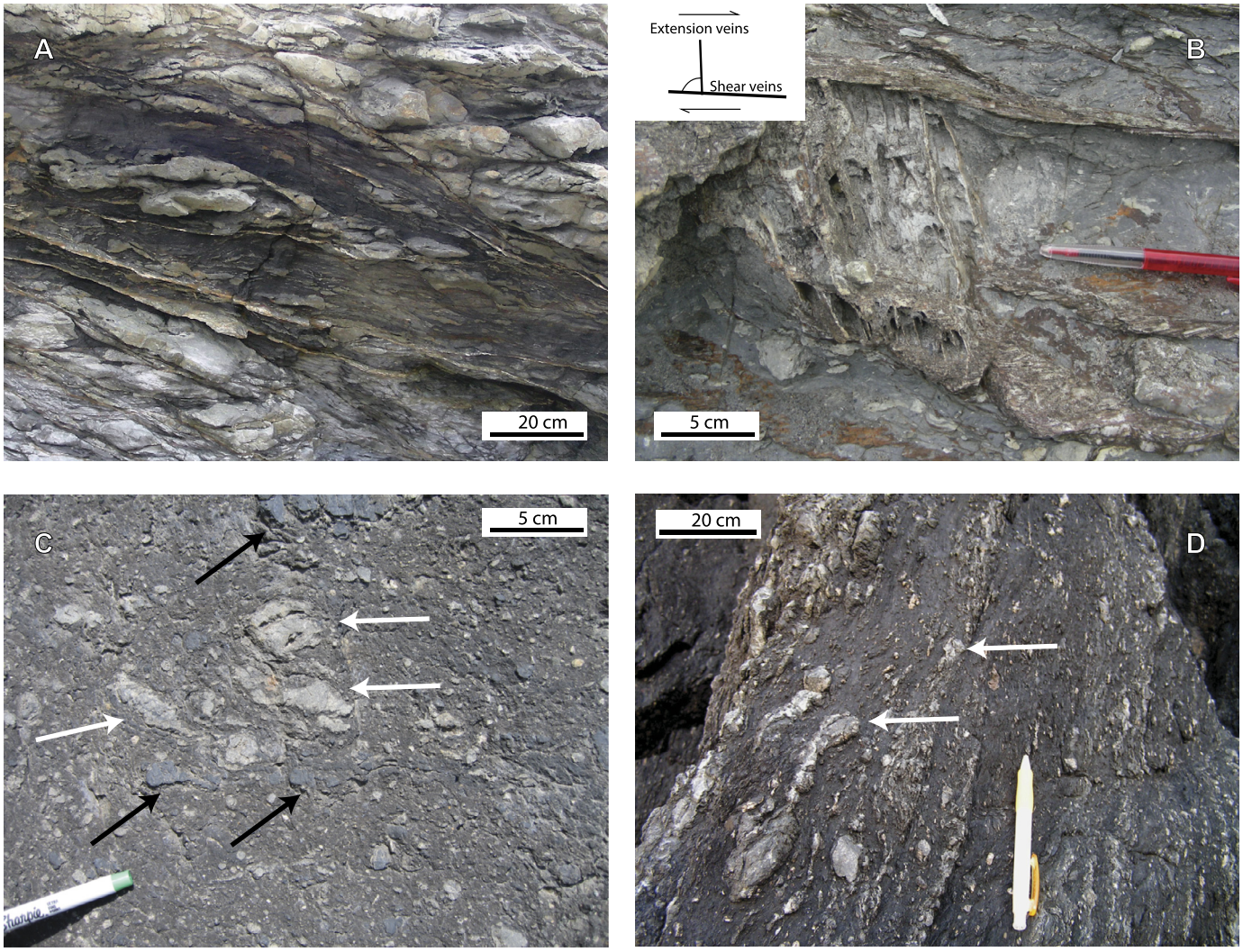

Fig. 9. Examples of outcrop structures associated with slow slip on subduction thrusts at seismogenic depths. (a) Mélange shear zone in the Chrystalls Beach Complex with sandstone lenses in foliated mudstone matrix deformed by pressure-solution creep (Fagereng and den Hartog, 2017, original image from Å. Fagereng, written comm., 2018). (b) Mutually cross-cutting extension veins and slickenfiber shear veins in Chrystalls Beach shear zone (Fagereng and Harris, 2014, original image from Å. Fagereng, written comm., 2018). (c) Non-foliated cataclasite indicative of accelerated aseismic or seismic slip in Pasagshak Point subduction thrust. White arrows point to sandstone clasts, black arrows indicate melt-bearing fault rock clasts indicative of coeval seismic slip. (d) Foliated and asymmetrically folded clast-rich cataclasite indicative of steady fault creep. Fabrics are self-similar over several orders of magnitude and reflect deformation of the mudstone matrix by pressure-solution creep (Rowe et al., 2011, original images from C. Rowe, written comm., 2018).

time-dependent state of asperity contacts. The state and frictional strength adjust to a new slip rate over a critical slip distance D_c, with empirical constants a and b describing the immediate and slip-dependent changes of friction, respectively (Fig. 12c and d, see Marone, 1998; Avouac, 2015 and many references therein). In a velocity-strengthening fault, an increase in sliding velocity will always lead to an increase in the steady-state coefficient of friction ($a > b$, Fig. 12c), and slip remains aseismic. Slow slip will also occur in a velocity-weakening fault, if the effective stiffness of the system is greater than a critical stiffness or, equivalently, if the slip zone is smaller than a critical patch size (h^*). In that case, with increasing slip, the elastic stress release exceeds the rate of frictional strength loss, thus stabilizing slip. In this slip-stability framework, model parameters inferred near the upper and lower regions of the seismogenic zone appear to favor the occurrence of slow slip and spontaneous SSEs. While rate-and-state friction models are empirical constructs, much effort has gone into illuminating the underlying mechanisms (Chen et al., 2017, and references cited therein) and exploring the factors producing the rich fault slip behavior observed in these models, in the laboratory and in nature.

The rate-and-state friction expressions underlie a large number of computational models of slow slip, earthquake nucleation and SSEs. Such models have explored the spatiotemporal evolution of slow slip through the earthquake cycle (Fig. 11; e.g., Barbot et al., 2012; Johnson et al., 2013; Avouac, 2015) and examined conditions for and the dynamics of SSEs (e.g., Liu and Rice, 2009; Segall et al., 2010). The competition of dynamic weakening (e.g., thermal pressurization) and strengthening (e.g., dilatancy) mechanisms in such models allows for destabilization and stabilization of fault slip, and there are conditions under which slip can transition between slow and seismic slip velocities in space and time (e.g., Chen and Lapusta, 2009; Shibazaki et al., 2011; Noda and Lapusta, 2013). Models that invoke heterogeneous frictional fault properties (Skarbek et al., 2012) may be appropriate to represent the variable materials, structures and slip modes found in many natural faults (see Sections 2 and 3) and considered in some laboratory experiments (see Section 4.2).

There are alternative approaches to rate-and-state friction when modeling slow slip. To capture the increasing contributions of viscous deformation processes near the brittle–ductile transition, Shimamoto and Noda (2014) develop a friction-to-flow model of a

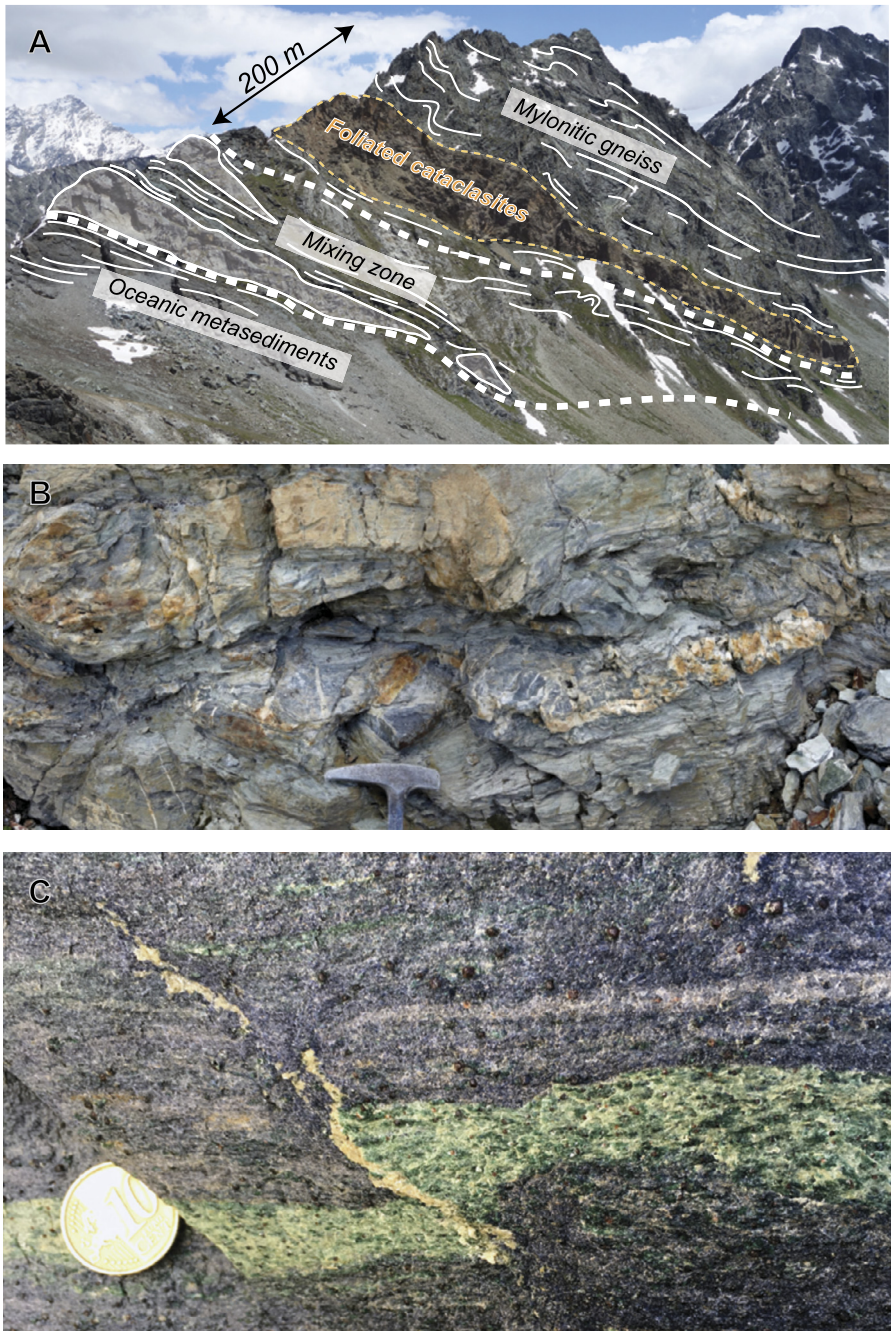

Fig. 10. Geologic examples of exhumed deep subduction thrusts suggested to have deformed by slow slip accompanied by tremor. (a) Alpine subduction thrust exhumed from 30–40 km depth, near Moiry Lake, Switzerland. Mylonitic granitic gneiss overlies an ~100-m-thick foliated cataclasite lens, intermixed continental and oceanic rocks, and ophiolitic metasediments (based on Angiboust et al., 2015). (b) Close-up of foliated cataclasite at Moiry Lake. Deformation involves grain-scale cataclasis of granitic gneiss, opening of several generations of quartz and epidote veins, mylonitic overprinting, and reorientation of veins (original image from S. Angiboust, written comm., 2017). (c) Dilational shear fracture filled with quartz offsetting a brittle eclogitic lens. The fracture is oriented at low angles to and merges into the foliation of the surrounding ductile blueschist matrix (original image from Behr et al., 2018).

fault zone with rate-state friction transitioning into a ductile shear zone with a power-law rheology. Ando et al. (2012) and Lavier et al. (2013) use alternative formulations with brittle and ductile fault rheologies to model transient slow slip and tremor in the transition regime. Yin et al. (2018) invoke a viscoplastic rheology of the transition zone to model deep-seated SSEs. Montesi (2004) shows that stress-driven afterslip on a velocity-strengthening fault zone is functionally similar to the case of a power-law fault rheology relating strain rate to stress with a very large power-law exponent n. To model lower-crustal SSEs and associated tremor characteristics, Ben-Zion (2012) employs a model of interacting cellular slip patches that have both ductile (power-law) and frictional properties. A viscoelastic damage rheology (Ben-Zion and Lyakhovsky, 2006) can also be used to represent fault zones that accommodate both seismic and aseismic strain.

4.2. Slow slip in the laboratory

Much of what we know about the mechanics of slow slip comes from experimental studies exploring the behavior of frictional fault surfaces and fault-zone materials over a range of loading and environmental conditions. Substantial effort has focused on establish-

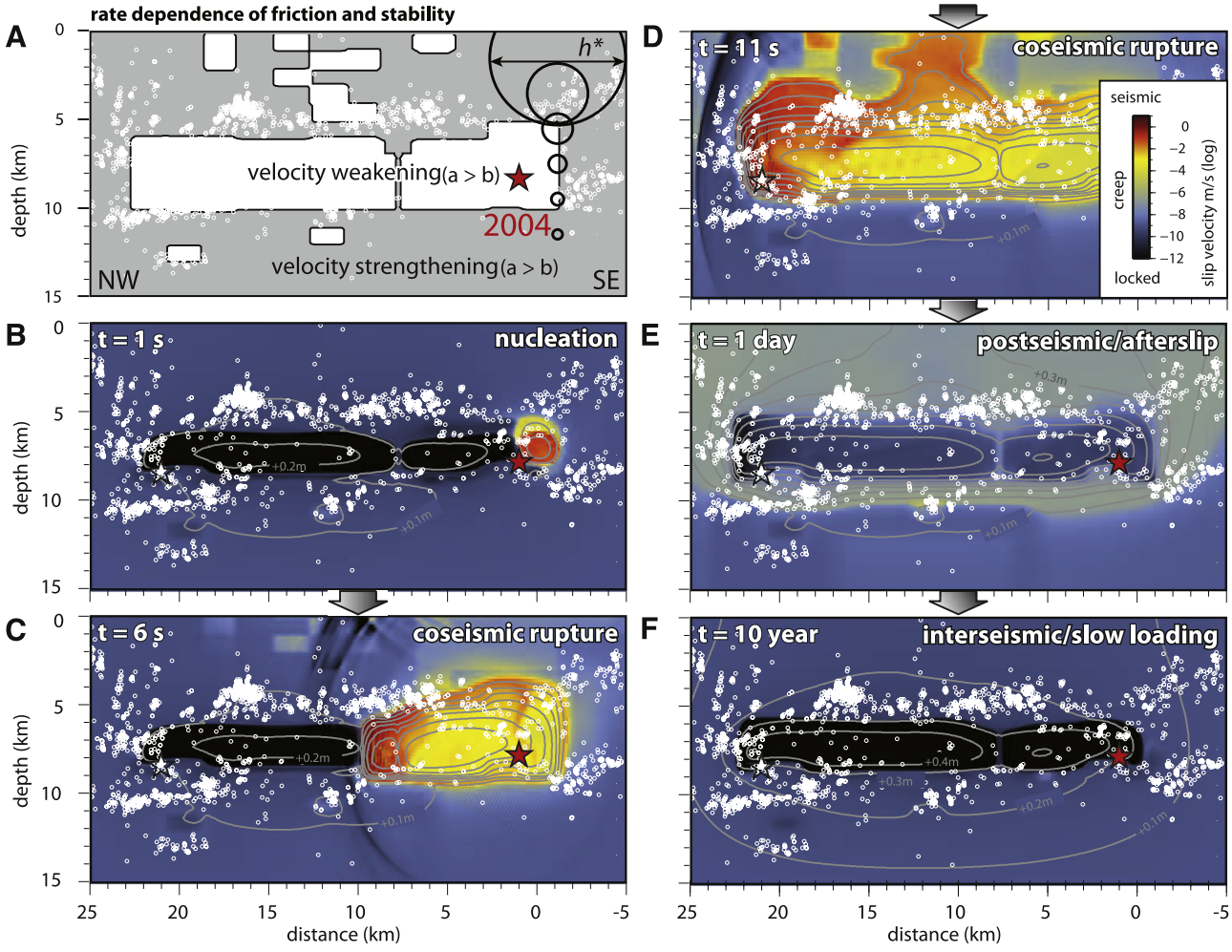

Fig. 11. Numerical rate-and-state friction model of the earthquake cycle on the partially coupled San Andreas fault at Parkfield (modified from Barbot et al., 2012). (a) Cross-section of the distribution of velocity-weakening (white) and velocity-strengthening (gray) frictional properties in the model. Black circles show the critical patch size (h^*) for unstable slip decreasing with depth. (b)–(f) Evolution of slip (gray contours of cumulative slip at 0.1-m intervals) and slip velocity (color contours) through the earthquake cycle. Rupture spontaneously nucleates near the hypocenter of the 2004 M 6 Parkfield earthquake (red star), dynamically propagates to the north, and is followed by aseismic afterslip away from the rupture that transitions into steady interseismic loading.

ing which materials offer increasing frictional resistance to rising sliding velocity and the factors and processes that stabilize fault slip (e.g., Marone, 1998). In recent years, laboratory experiments have explored a wider range of fault-zone materials and properties and considered variable experimental conditions, geometry and scale.

Experiments aimed at shallow fault properties find that unconsolidated clay-rich fault materials exhibit velocity-strengthening behavior, over a wide range of compositions indicative of dilation strengthening in granular materials (Ikari et al., 2009; Saffer et al., 2012). Certain minerals, including some clays, serpentine minerals and talc, are found to be velocity strengthening in the laboratory over a wide range of conditions, suggesting that composition alone can promote slow slip over temperature and depth ranges at which these materials are stable (Moore and Rymer, 2007; Lockner et al., 2011). Ikari and Kopf (2017) describe experiments on weak clay-rich fault samples collected by shallow drilling from seven plate-boundary faults. When they sheared samples at very low slip velocities consistent with steady tectonic loading (~nm/s), they found unstable slip and SSEs, even though most of those samples were velocity-strengthening at the much higher sliding rates (~μm/s) that are usually applied in such experiments. These findings are consistent with recent geophysical evidence of shallow earthquake ruptures and SSEs described in Section 2, which require a weakening mechanism to allow such instabilities to initiate.

Other experiments find that faults can exhibit bimodal (either fast or slow) slip behavior due to the activation of diverse weakening or strengthening processes by strong variations in slip speed. For example, a velocity strengthening fault can become unstable at high slip rates due to dynamic weakening processes (e.g., Kohli et al., 2011, and references cited therein), suggesting that it is possible for a dynamic rupture to break through an otherwise creeping section of a fault. On the other hand, slip acceleration can also produce dilatant strengthening, putting the brakes on fault slip and leading to velocity-strengthening behavior (Kaproth and Marone, 2013). Kaproth and Marone (2013) also find seismic wave speed reduction in a serpentinite fault zone accompanying slow slip, indicating dilatant processes associated with precursory slow slip. Experiments in which fluid pressure is controlled in experimental faults show that rising fluid pressure can both stabilize and destabilize fault slip through the effects of competing compaction and dilation processes on fluid flow, pressure and frictional strength during sliding (e.g., Scuderi et al., 2017; Faulkner et al., 2018). Experiments conducted at hydrothermal conditions approaching the brittle–ductile transition of crustal rocks find that inferred rate-and-state frictional fault properties are strongly dependent on sample mineralogy and associated plastic

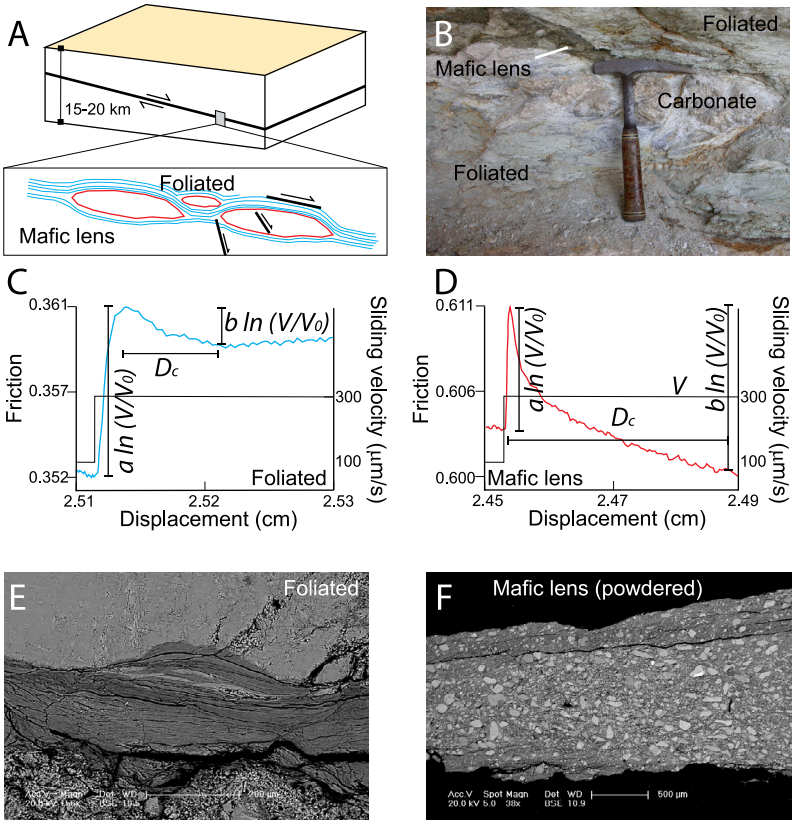

Fig. 12. Slow and fast slip in the heterogeneous Zuccale fault zone on Elba Island, Italy (based on Collettini et al., 2011; original images from C. Collettini, written comm., 2018). (a) Schematic view and (b) photograph of the Zuccale Fault containing foliated phyllosilicate-rich layers surrounding stronger lenses of mafic and carbonate material. Velocity-step experiments on (c) frictionally weak and velocity-strengthening ($a > b$) foliated material and (d) strong and velocity-weakening ($a < b$) mafic lens material. Corresponding micrographs of (e) phyllosilicate-rich foliated sample fault and (f) powdered mafic fault material used for the experimental results in (c) and (d).

and pressure-solution deformation mechanisms (He et al., 2013). More work exploring the mechanical and chemical effects of fluids and temperature will be needed to better understand the various processes and factors involved in this behavior.

In laboratory experiments on modestly velocity-weakening faults, a finite SSE will develop if the slip patch size remains within a critical dimension (h^*) related to the effective stiffness of the loading system (see section 4.1). In this case, elastic stress decays more rapidly than the frictional strength, preventing dynamic acceleration. In experiments where the system stiffness is near the transition value separating stable and unstable behavior, complex transient slow slip behavior can be produced (e.g., Leeman et al., 2016). McLaskey and Kilgore (2013) explore friction experiments on meter-scale samples larger h^* and find that small foreshocks in the slow slip zone accompany the slow nucleation phase before the experimental mainshock. Very high stressing rates during the slow slip period may trigger such small asperity failures, which are reminiscent of precursory earthquake swarms and SSEs observed prior to some earthquake ruptures. Using a sample that is sized close to the critical nucleation dimension, McLaskey and Yamashita (2017) find that faulting can be made to switch from aseismic to seismic slip simply by rapidly increasing the loading rate. They suggest that this could explain the transition from tremorogenic to silent slow slip found by Wech and Bartlow (2014, see Fig. 5c) and the emergence or magnitude increases of repeating earthquakes and LFEs during afterslip episodes (Chen et al., 2010; Veedu and Barbot, 2016; Hatakeyama et al., 2017).

Natural faults often feature discontinuities and irregular surface morphology and contain heterogeneous materials, such as more competent lenses of rocks with different composition or metamorphic grade (see Section 3). Harbord et al. (2017) explore the role of fault-surface roughness and find that a combination of roughness and normal stress influences the stable or unstable accommodation of slip, with rougher fault surfaces favoring slow slip. They suggest that their results qualitatively support the idea that rough seafloor topography entering subduction zones promotes creeping subduction thrust behavior (Wang and Bilek, 2014). A foliated fault gouge fabric and contribution of pressure-solution creep in multimineralic fault-zone materials also promote velocity-strengthening behavior (e.g., Niemeijer and Spiers, 2006; Collettini et al., 2009; Collettini et al., 2011). The highly heterogeneous frictional properties deduced from laboratory experiments of field samples from such fault zones (Fig. 12) suggest mixed-mode behavior with coexisting slow slip and seismic events (e.g., Collettini et al., 2011, and references cited there). It is difficult for small-scale experiments (Pec et al., 2016) to fully capture the heterogeneous structures and multiple deformation processes found in natural fault zones (e.g., Figs. 8–10). Results from larger-scale experiments involving semi-brittle rock analogue materials (Reber et al., 2015) suggest that the interaction of viscous flow and a system of tensional and shear fractures can produce fault-zone structures and slip behaviors resembling those observed in such heterogeneous natural fault zones.

In summary, as laboratory scientists consider a more diverse set of experimental parameters, inspired by geophysical and geological observations, they find more complex and diverse fault-zone behaviors that are not always captured by existing theoretical frameworks. These results suggest that spatial and temporal changes in conditions (e.g., composition, micro-structure, fluid pressure, and slip rate) found in natural fault systems are likely to promote spatial and temporal variations in the occurrence of slow slip.

4.3. Slow slip in the natural laboratory

Ideally, we can explore the mechanics of slow slip on natural faults, by closely studying their response to manmade or natural changes in boundary conditions. There is evidence of induced slow slip associated with triggered seismicity due to injection of wastewater near preexisting faults (Duboeuf et al., 2017 and references cited therein). Bourouis and Bernard (2007) find sequences of repeating micro-earthquakes on faults near an active injection site in Soultz, France, at ∼3 km depth indicative of slow slip initiated by fluid pressure increases. Induced creep of up to ∼0.2 m was distributed on a ∼400-m wide fault, illuminated by the repeaters. Guglielmi et al. (2015) and Duboeuf et al. (2017) carried out field experiments in which rapid fluid injections induced aseismic fault slip that was associated with induced microseismicity. Comparison of the slip measurements, relying on what is effectively a 3D borehole creepmeter, and seismic moment release suggests that most of the induced deformation is aseismic (Duboeuf et al., 2017). Considering lab experiments, modeling and seismological observations, Zoback et al. (2012) conclude that slow slip, either from fluid pressure increases and/or from high clay content in the fault zone material, is an important deformation mechanism associated with shallow hydraulic fracturing. Consistent with laboratory and computational models, these natural-laboratory experiments suggest that decreased effective normal stress in a fault zone may lead to slow slip, while also stimulating induced seismicity.

Examples of natural experiments illuminating slow-slip mechanics include slow slip accelerations induced by coseismic stress changes and tidal modulation of slow slip. Hatakeyama et al. (2017) examine the changing character of small repeating earthquakes located in the afterslip zone of the 2011 Tohoku-oki (Fig. 5). They find that the accelerated loading rates during the afterslip transient caused systematic increases in magnitude and slip area of repeating earthquakes and allowed patches on the plate interface, which had slipped aseismically in previous decades, to repeatedly slip in small earthquakes. As afterslip rates decayed, so did the size of the repeating earthquakes and the emergent seismic sources started to disappear again. These results are consistent with similar observations following the 2004 Parkfield earthquake and numerical rate-and-state friction models that predict such variable slip behavior for small velocity-weakening fault patches embedded in a velocity-strengthening fault zone (Chen et al., 2010).

The response of creeping, tremor-producing fault zones near the brittle–ductile transition to tidal stress cycles represents another example of a natural slow-slip experiment (Hawthorne and Rubin, 2010; Thomas et al., 2012). Beeler et al. (2013b) examine the response of low-frequency earthquakes to very small ($<\pm$300 Pa) tidal shear-stress changes (Thomas et al., 2012) to argue that rate-dependent friction at extremely low effective normal stress could explain the observed correlation, while aseismic shearing of the fault zone by dislocation creep or other ductile deformation mechanisms cannot. Houston (2015) find that the correlation of tremor occurrence and tidal stress on the Cascadia subduction thrust becomes stronger as slow slip accumulates during an SSE. This suggests that the subduction thrust has both an intrinsically low coefficient of friction and near-lithostatic fluid pressure, and that the fault further weakens with ensuing transient slow slip. The observation that tremors strongly respond to tides while regular earthquakes do not appears consistent with the frequency-dependent frictional response of laboratory faults to oscillatory loads at high fluid pressures (Bartlow et al., 2012). Improved seismologic and geodetic monitoring of natural creeping faults should allow for many more of these natural-laboratory experiments and improved understanding of the mechanics of slow slip.

5. Discussion and new frontiers of slow-slip research

5.1. The ingredients of slow slip

There are a number of successful recipes for slow fault slip, SSEs and tremor. Based on the geophysical, geological, and modeling insights discussed above, good ingredients for fault creep are: (1) a velocity-strengthening fault zone material (many available mixes of clays and other phyllosilicates will do, especially if they are arranged in a continuous foliated fabric), and/or (2) modestly velocity-weakening fault patches that are smaller than a critical dimension needed for earthquake nucleation, and/or (3) abundant fluids at high pressure, and/or (4) high fault roughness and heterogeneous fault structure and composition over a wide range of scales. If all else fails, increasing temperature and pressure to a level at which some of the fault-zone material is ductile should produce aseismic slip in a weakened mylonitic shear zone. Adding water almost always helps, as the chemical reactions and mechanical processes that fluids facilitate generally favor slow slip and weaken faults. Beware, stirring up a fault too rapidly or very slowly can destabilize the slip and result in an earthquake.

To make a slow earthquake with a velocity-strengthening fault is difficult. A velocity-weakening fault patch that has a dimension small enough, or stiffness high enough, so that the load stress decays more rapidly than the frictional fault strength is better for producing an SSE. High fluid pressure has been found to help in this effort. Making an SSE also benefits from dilatant fracturing, as this helps quench the fault slip and prevent runaway failure. However, as for slow slip in general, suddenly increasing water pressure or slip rate can sufficiently weaken a fault to induce unstable seismic fault slip. If we also want our fault to provide a taste of tremor (i.e., a little but not too much seismic slip in places), we may need especially high fluid pressure to hold open cracks against the lithostatic stress and a fault-zone mix that is spatially variable in composition or metamorphic grade.

5.2. The strength of aseismic faults

Just because a fault slips slowly does not mean that it supports less stress than its seismogenic counterpart. While the frictional strength of most rocks is found to be high (Byerlee and Brace, 1968), intrinsically low-friction materials, dynamic weakening mechanisms, and high fluid pressure may leave both seismic and aseismic natural faults to be much weaker. Nonetheless, laboratory experiments find that low-friction materials, such as some phyllosilicates, also tend to be velocity-strengthening, while stronger fault-zone materials exhibit both stable and unstable slip (e.g., Ikari and Kopf, 2017).

Geophysical measurements of stress orientations and heat flow suggest that both strike-slip and subduction plate boundary faults may not support more than a few 10s-of-MPa shear stress. However, there has been debate about if creeping faults are weaker than seismogenic ones (e.g., Hardebeck and Michael, 2004; d'Alessio et al., 2006; Gao and Wang, 2014; Hardebeck and Loveless, 2018). For example, heat flow data suggest that megathrusts that host great earthquakes tend to be weaker than largely uncoupled sections (Gao and Wang, 2014). On the other hand, stress inversion data indicate that creeping subduction thrusts have lower effective friction coefficients than the, still quite weak, locked regions (Hardebeck and Loveless, 2018).

At the scale of plate boundary faults, not only the intrinsic frictional properties of fault-zone materials and fluid pressure, but also the larger-scale structure and combination of seismic and aseismic deformation processes determine the effective strength of a fault (e.g.,Wang and Bilek, 2014). Slow-slipping faults that also

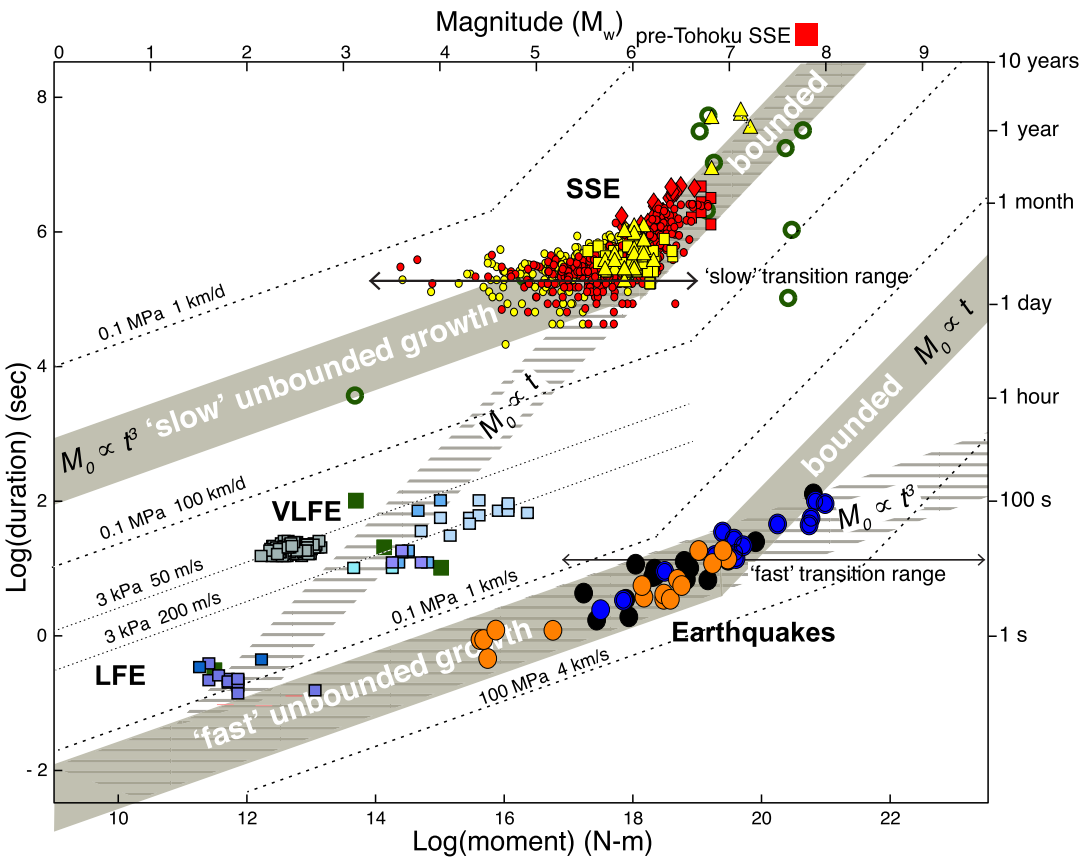

Fig. 13. Moment (M_o) versus duration (t) of seismic and aseismic slip events and proposed scaling relationships (simplified from Gomberg et al., 2016). See Gomberg et al. (2016) for source event information about the SSEs, very-low-frequency earthquakes (VLFE), low-frequency earthquakes (LFE), and earthquakes shown in various colors and symbols. Transitions from unbounded to bounded slip dimensions roughly correspond to transitions from $n \approx 3$ to $n \approx 1$ in the scaling relationship $M_o \propto t^n$. Dashed and dotted lines denote representative stress drops and rupture propagation velocities for the different event types. SSEs have several orders of magnitude lower stress drops (~50 kPa) than earthquakes (~5 MPa).

produce tremor appear to be especially weak and are easily triggered to slip by very low stress changes from nearby earthquakes, dynamic shaking, or tidal stresses (see Section 4.3). This may be explained by the combined effect of intrinsically low-friction fault materials, near-lithostatic fluid pressure, and abundant fluid-filled fractures in the fault zone (e.g., Hawthorne and Rubin, 2010; Thomas et al., 2012; Houston, 2015; Beeler et al., 2018).

5.3. The thickness of creeping faults

The width of a creeping fault zone determines the strain rate, and thus the dominant deformation processes accommodating slow slip (Fig. 1). As fault zone composition, brittle structures (e.g., tensile and shear fractures) and ductile deformation mechanisms (e.g., pressure-solution and dislocation creep) all contribute, slow slip need not reflect displacement on a single or few discrete fault surfaces. Shallow creeping faults near the Earth's surface are usually very narrow (Figs. 2 and 8). Enduring repeating micro-earthquake sequences, driven to failure by surrounding slow slip in strike-slip and thrust environments (Fig. 4A and 5A), are indicative of the actively creeping fault remaining quite thin across the seismogenic zone. Similarly, the recurrence of effectively collocated low-frequency and very-low-frequency earthquakes in deep, tremor-producing fault zones, and the ease with which large-scale SSEs propagate over hundreds of km (Fig. 5c) suggests quite localized fault creep. Geophysical imaging and geologic studies suggest that the thickness of fault damage zones and zones of high fluid content increases with depth from 100s of m to several km (Figs. 6 and 7). However, active fault strands within such zones may be more localized in m- to 10s-of-m wide shear zones (Figs. 9 and 10, Rowe et al., 2013). Careful consideration of micro- and macro-scale geological, geophysical and laboratory observations will be needed to better understand the structures accommodating slow slip of actively creeping faults from top to bottom.

5.4. The wide spectrum of fault slip events

With improving temporal resolution and accuracy of geodetic and seismic observations, it has become apparent that slow slip involves transients with a wide range of sizes, recurrence intervals and durations at all depths (Peng and Gomberg, 2010). SSEs distinguish themselves from earthquakes by their orders-of-magnitude lower slip rates, propagation velocities and stress drops, and much longer event durations. A systematic scaling between slip-event magnitude (expressed as seismic moment M_o) and duration (t) has been proposed, $M_o \propto t^n$, where n appears to be about three for fast seismic events and approaches one for SSEs (e.g., Ide et al., 2007). Gomberg et al. (2016), however, find that the scaling for both fast and slow events appears to transition from $n = 3$ to $n = 1$ in this relationship, as slip patches reach the up- and down-dip boundaries of their respective slip zone, thus changing from unbounded to bounded slip (Fig. 13). To date, the largest documented SSEs have been of equivalent moment magnitude of about M_w 7.2; however, Meade and Loveless (2009) argue that changes in seismic coupling at decadal time scales may represent long-lasting, $M_w \approx 8$ SSEs. Mavrommatis et al. (2015) used GNSS time series and repeating earthquake data to document accelerating slow slip rates on the subduction thrust in northeast

Japan over a 15-year period preceding the 2011 Tohoku-oki earthquake, with added moment release during this time equivalent to an M_w 7.7 event (A. Mavrommatis, 2017, pers. comm., red square in Fig. 13). This suggests that the spatial and temporal scales of SSEs may indeed be quite open ended. More observational and theoretical work will be needed to establish to what degree the wide spectrum of tremor and SSE behaviors can be described in a consistent mechanical framework (Hawthorne and Bartlow, 2018; Ide and Maury, 2018).

5.5. Slow slip, the earthquake cycle and earthquake hazard

Better understanding of slow slip during all phases of the earthquake cycle should allow for improved earthquake hazard assessment. Relatively steady interseismic creep below the seismogenic zone strongly contributes to the overall stress build up leading to eventual earthquake ruptures. Thus, model estimates of deep slip rates form an important ingredient of long-term hazard assessments (Field et al., 2014). Fault creep at seismogenic depths reduces a fault's overall seismic potential, but not necessarily the ground motion of earthquakes on partially coupled faults (Field et al., 2014; Harris, 2017). Slip accelerations or SSEs during the interseismic phase of the earthquake cycle produce transient stress increases on nearby locked patches that temporarily increase earthquake probabilities (e.g., Mazzotti and Adams, 2004; Shirzaei et al., 2013). For example, stress and earthquake hazard on the Cascadia megathrust are raised (Mazzotti and Adams, 2004) during each episode of slow slip and tremor below the locked zone (Fig. 5c). However, the earthquake-probability increases during these recurring SSEs are probably modest (Beeler et al., 2013a). On the other hand, it is possible that a "runaway SSE" propagating further up dip than usual, becomes the nucleation phase of an eventual great megathrust earthquake (Segall and Bradley, 2012), motivating continuous monitoring of slow slip in space and time.

Precursory SSEs and associated foreshock sequences have preceded some large earthquakes (Fig. 7, Roeloffs, 2006; Kato et al., 2012; Meng et al., 2015; Radiguet et al., 2016; Socquet et al., 2017). The durations of these precursory slip transients range from seconds to years and their slip areas and inferred slip also span a wide range (Roeloffs, 2006). The preseismic slip often occurs adjacent to the coseismic rupture, rather than within the eventual nucleation zone and rupture. While a direct correlation between slow slip accelerations and some larger earthquakes can be documented (e.g., Uchida et al., 2016), most SSEs occur without subsequent large earthquakes. Thus, rather than being an inherent part of the earthquake-nucleation process, the association of SSEs with subsequent earthquake ruptures may simply reflect triggering relationships similar to those between earthquakes (Freed, 2005). While improved observations of slow slip are not likely to lead to reliable short-term earthquake predictions, refined characterization of slow slip episodes and their relation to large earthquakes continues to be a promising area of research (Obara and Kato, 2016).

Postseismic slow slip comes in two flavors. Stress-driven afterslip relieves coseismic stress increases on nearby fault sections that are capable of slow slip (Figs. 4, 5a, b and 11e, Ingleby and Wright, 2017 and references cited therein). Static and dynamic stresses from a mainshock rupture can also lead to triggered postseismic SSEs relieving stress that had already built up during the preceding inter-SSE period (Fig. 3c, Taira et al., 2014; Araki et al., 2017; Wallace et al., 2017; Rolandone et al., 2018). Together with other postseismic relaxation mechanisms, slow slip of either type can enhance static stress changes at large distances from a mainshock and trigger subsequent events (e.g., Hearn et al., 2002; Freed, 2005).

5.6. New frontiers of slow-slip research

Recent advances in the understanding of slow slip from geophysical, geological and modeling studies described in Sections 2 through 4 point the way to future interdisciplinary investigations. It seems particularly important to further integrate evidence from multiple geophysical techniques, complementary geologic outcrops, and experimental and computational models. Below are a few examples of promising and challenging targets of future slow slip research.

As most seismic and aseismic moment release occurs below the sea floor, geophysical seafloor observations will greatly enhance slow-slip research. Given the recent success of such observations in global subduction zones (Figs. 3 and 5, Wallace et al., 2016; Yokota et al., 2016; Araki et al., 2017), these most hazardous plate-boundary fault systems justifiably are top-priority targets for future research (McGuire et al., 2017). Recent studies of precursory earthquake swarm activity and reduced seismic velocities in the Gofar transform fault (see Fig. 7, McGuire et al., 2012) and the discovery of repeating earthquakes driven by slow slip on the Mendocino transform fault (Materna et al., 2018) point to oceanic transform faults also being great targets for future integrated seafloor geodetic and seismologic investigations of slow slip.

Much progress has been made in finding exhumed fault zones that provide new insights on the environment, structures and processes of slow slip. The integration of observations from the thin-section to regional outcrop scale with laboratory experiments on samples collected from such sites (e.g., Fig. 12), illuminates the role of multiple deformation processes and structures producing slow slip. Geophysical and modeling studies should explicitly consider the constraints provided by these geologic studies, while geologists should formulate their hypotheses in the context of geodetic and seismologic phenomena (e.g., the spatial and temporal scales of slow slip and associated seismic activity, Figs. 4 and 5) and geophysical constraints on the environment of slow slip (e.g., Figs. 6 and 7).

Important frontiers in experimental research lie in further explorations of the roles of scale and water. Better understanding the roles of slip patch dimension, heterogeneous fault zone composition, fault-surface morphology, and secondary structures requires larger-scale experiments or well-designed natural-laboratory investigations. Ideally, experimental studies should be accompanied by computational models that allow for examining the degree to which experimental insights can be scaled to the spatial and temporal scales of natural systems. Crustal fluids and the spatio-temporal variability of fluid pressure play a fundamental role in fault behavior and the occurrence of earthquakes and slow slip (Sibson, 2017). Fluids influence faults through the magnitude of effective normal stress, the development of fluid filled fractures, chemical reactions and phase transitions, and the activation of pressure-solution creep and plastic deformation mechanisms. Increasing fluid pressure can both stabilize and destabilize fault slip. Future experiments should aim to more fully illuminate the mechanisms and consequences of fluid effects on active faulting.

Finally, slow slip also plays an important role in the mechanics of landslides (e.g., Handwerger et al., 2016), glaciers (e.g., Lipovsky and Dunham, 2017) and volcanoes (e.g., Dmitrieva et al., 2013). Studies of slow slip in these systems is likely to improve our understanding of the behavior and hazard of tectonic faults, and vice versa.

Acknowledgements

I thank everybody who provided figures and/or helpful discussions and thoughtful comments during the preparation of this review, including Samuel Angiboust, Pascal Audet, Sylvain Barbot,

Noel Bartlow, Michael Becken, Nick Beeler, Whitney Behr, Goetz Bokelmann, Kate Huihsuan Chen, Cristiano Collettini, Ake Fagereng, Joan Gomberg, Nick Hayman, Mong-Han Huang, Kaj Johnson, Romain Jolivet, Jamie Kirkpatrick, Thorne Lay, Kathryn Materna, Andreas Mavrommatis, Jeff McGuire, Greg McLaskey, Francois Renard, Christie Rowe, Manoo Shirzaei, Rick Sibson, Marion Thomas, Cliff Thurber, Ryan Turner, Laura Wallace, Aaron Wech, An Yin, Yosuke Yokota, Xiangfang Zeng, and Mark Zoback. Whitney Behr, Laura Wallace and an anonymous reviewer are thanked for their constructive reviews; Whitney inspired Table 2.

References

Ambraseys, N.N., 1970. Some characteristic features of the Anatolian Fault zone. Tectonophysics 9, 143–165. https://doi.org/10.1016/0040-1951.

Anderlini, L., Serpelloni, E., Belardinelli, M.E., 2016. Creep and locking of a low-angle normal fault: insights from the Altotiberina fault in the Northern Apennines (Italy). Geophys. Res. Lett. 43, 4321–4329. https://doi.org/10.1002/2016GL068604.

Ando, R., Takeda, N., Yamashita, T., 2012. Propagation dynamics of seismic and aseismic slip governed by fault heterogeneity and Newtonian rheology. J. Geophys. Res., Solid Earth 117. https://doi.org/10.1029/2012JB009532.

Angiboust, S., Kirsch, J., Oncken, O., Glodny, J., Monie, P., Rybacki, E., 2015. Probing the transition between seismically coupled and decoupled segments along an ancient subduction interface. Geochem. Geophys. Geosyst. 5, 1905–1922. https://doi.org/10.1002/2015GC005776.

Araki, E., Saffer, D.M., Kopf, A.J., Wallace, L.M., Kimura, T., Machida, Y., Ide, S., Davis, E., 2017. Recurring and triggered slow-slip events near the trench at the Nankai Trough subduction megathrust. Science 356, 1157. https://doi.org/10.1126/science.aan3120.

Audet, P., Bürgmann, R., 2014. Possible control of subduction zone slow-earthquake periodicity by silica enrichment. Nature 510, 389–392. https://doi.org/10.1038/nature13391.

Audet, P., Kim, Y., 2016. Teleseismic constraints on the geological environment of deep episodic slow earthquakes in subduction zone forearcs: a review. Tectonophysics 670, 1–15. https://doi.org/10.1016/j.tecto.2016.01.005.

Audet, P., Schaeffer, A.J., 2018. Fluid pressure and shear zone development over the locked to slow slip region in Cascadia. Sci. Adv. 4, eaar2982. https://doi.org/10.1126/sciadv.aar2982.

Audet, P., Schwartz, S.Y., 2013. Hydrologic control of forearc strength and seismicity in the Costa Rican subduction zone. Nat. Geosci. 6, 852–855. https://doi.org/10.1038/ngeo1927.

Avouac, J.P., 2015. From geodetic imaging of seismic and aseismic fault slip to dynamic modeling of the seismic cycle. Annu. Rev. Earth Planet. Sci. 43, 233–271. https://doi.org/10.1146/annurev-earth-060614-105302.

Barbot, S., Lapusta, N., Avouac, J.-P., 2012. Under the hood of the earthquake machine: toward predictive modeling of the seismic cycle. Science 336, 707–710. https://doi.org/10.1126/science.1218796.

Bartlow, N.M., Lockner, D.A., Beeler, N.M., 2012. Laboratory triggering of stick–slip events by oscillatory loading in the presence of pore fluid with implications for physics of tectonic tremor. J. Geophys. Res., Solid Earth 117. https://doi.org/10.1029/2012JB009452.

Bartlow, N.M., Miyazaki, S.I., Bradley, A.M., Segall, P., 2011. Space–time correlation of slip and tremor during the 2009 Cascadia slow slip event. Geophys. Res. Lett. 38. https://doi.org/10.1029/2011GL048714.

Bassett, D., Sutherland, R., Henrys, S., 2014. Slow wavespeeds and fluid overpressure in a region of shallow geodetic locking and slow slip, Hikurangi subduction margin, New Zealand. Earth Planet. Sci. Lett. 389, 1–13. https://doi.org/10.1016/j.epsl.2013.12.021.

Becken, M., Ritter, O., Bedrosian, P.A., Weckmann, U., 2011. Correlation between deep fluids, tremor and creep along the central San Andreas fault. Nature 480, 87–90. https://doi.org/10.1038/nature10609.

Bedrosian, P.A., Unsworth, M.J., Egbert, G.D., Thurber, C.H., 2004. Geophysical images of the creeping segment of the San Andreas fault: implications for the role of crustal fluids in the earthquake process. Tectonophysics 385, 137–158. https://doi.org/10.1016/j.tecto.2004.02.010.

Beeler, N.M., Lockner, D.L., Hickman, S.H., 2001. A simple stick–slip and creep–slip model for repeating earthquakes and its implications for microearthquakes at Parkfield. Bull. Seismol. Soc. Am. 91, 1797–1804.

Beeler, N.M., Roeloffs, E.A., McCausland, W., 2013a. Re-estimated effects of deep episodic slip on the occurrence and probability of great earthquakes in Cascadia. Bull. Seismol. Soc. Am. 104, 128–144. https://doi.org/10.1785/0120120022.

Beeler, N.M., Thomas, A., Bürgmann, R., Shelly, D., 2013b. Inferring fault rheology from low-frequency earthquakes on the San Andreas. J. Geophys. Res. 118, 5976–5990. https://doi.org/10.1002/2013JB010118.

Beeler, N.M., Thomas, A.M., Bürgmann, R., Shelly, D.R., 2018. Constraints on friction, dilatancy, diffusivity, and effective stress from low-frequency earthquake rates on the deep San Andreas Fault. J. Geophys. Res., Solid Earth 123, 583–605. https://doi.org/10.1002/2017JB015052.

Behr, W.M., Kotowski, A.J., Ashley, K.T., 2018. Dehydration-induced rheological heterogeneity and the deep tremor source in warm subduction zones. Geology 46 (5), 475–478. https://doi.org/10.1130/G40105.1.

Bell, R., Sutherland, R., Barker, D.H.N., Henrys, S., Bannister, S., Wallace, L., Beavan, J., 2010. Seismic reflection character of the Hikurangi subduction interface, New Zealand, in the region of repeated Gisborne slow slip events. Geophys. J. Int. 180, 34–48. https://doi.org/10.1111/j.1365-246X.2009.04401.x.

Ben-Zion, Y., 2012. Episodic tremor and slip on a frictional interface with critical zero weakening in elastic solid. Geophys. J. Int. 189, 1159–1168.

Ben-Zion, Y., Lyakhovsky, V., 2006. Analysis of aftershocks in a lithospheric model with seismogenic zone governed by damage rheology. Geophys. J. Int. 165, 197–210. https://doi.org/10.1111/j.1365-246X.2006.02878.x.

Beroza, G.C., Ide, S., 2011. Slow earthquakes and nonvolcanic tremor. Annu. Rev. Earth Planet. Sci. 39, 271–296. https://doi.org/10.1146/annurev-earth-040809-152531.

Beroza, G.C., Jordan, T.A., 1990. Searching for slow and silent earthquakes using free oscillations. J. Geophys. Res., Solid Earth 95, 2485–2510. https://doi.org/10.1029/JB095iB03p02485.

Bilham, R., Suszek, N., Pinkney, S., 2004. California creepmeters. Seimol. Res. Lett. 75, 481–492.

Bird, P., Kagan, Y.Y., 2004. Plate-tectonic analysis of shallow seismicity: apparent boundary width, beta, corner magnitude, coupled lithosphere thickness, and coupling in seven tectonic settings. Bull. Seismol. Soc. Am. 94, 2380–2399. arXiv:2310.1785/0120030107.

Blanpied, M.L., Lockner, D.A., Byerlee, J.D., 1991. Fault stability inferred from granite sliding experiments at hydrothermal conditions. Geophys. Res. Lett. 18, 609–612.

Bokelmann, G.H.R., Kovach, R.L., 2003. Long-term creep-rate changes and their causes. Geophys. Res. Lett. 30. https://doi.org/10.1029/2003GL017012.

Bourouis, S., Bernard, P., 2007. Evidence for coupled seismic and aseismic fault slip during water injection in the geothermal site of Soultz (France), and implications for seismogenic transients. Geophys. J. Int. 169, 723–732. https://doi.org/10.1111/j.1365-246X.2006.03325.x.

Brodsky, E.E., Lay, T., 2014. Recognizing foreshocks from the 1 April 2014 Chile earthquake. Science 344, 700–702. https://doi.org/10.1126/science.1255202.

Bürgmann, R., Chadwell, C.D., 2014. Seafloor geodesy. Annu. Rev. Earth Planet. Sci. 42, 509–534. https://doi.org/10.1146/annurev-earth-060313-054953.

Bürgmann, R., Dresen, G., 2008. Rheology of the lower crust and upper mantle: evidence from rock mechanics, geodesy and field observations. Annu. Rev. Earth Planet. Sci. 36, 531–567. https://doi.org/10.1146/annurev.earth.36.031207.124326.

Bürgmann, R., Rosen, P.A., Fielding, E.J., 2000. Synthetic aperture radar interferometry to measure Earth's surface topography and its deformation. Annu. Rev. Earth Planet. Sci. 28, 169–209. https://doi.org/10.1146/annurev.earth.28.1.169.

Byerlee, J.D., Brace, W.F., 1968. Stick slip, stable sliding, and earthquakes—effect of rock type, pressure, strain rate, and stiffness. J. Geophys. Res., Solid Earth 73, 6031–6037. https://doi.org/10.1029/JB073i018p06031.

Carpenter, B.M., Marone, C., Saffer, D.M., 2011. Weakness of the San Andreas Fault revealed by samples from the active fault zone. Nat. Geosci. 4, 251. https://doi.org/10.1038/ngeo1089.

Cashman, S.M., Baldwin, J.N., Cashman, K.V., Swanson, K., Crawford, R., 2007. Microstructures developed by coseismic and aseismic faulting in near-surface sediments, San Andreas fault, California. Geology 35, 611.

Chaussard, E., Bürgmann, R., Fattahi, H., Johnson, C.W., Nadeau, R., Taira, T., Johanson, I., 2015. Interseismic coupling and refined earthquake potential on the Hayward-Calaveras fault zone. J. Geophys. Res. 120. https://doi.org/10.1002/2015JB012230.

Chen, J., Niemeijer, A.R., Spiers, C.J., 2017. Microphysically derived expressions for rate-and-state friction parameters, a, b, and D_c. J. Geophys. Res. 122, 9627–9657. https://doi.org/10.1002/2017JB014226.

Chen, K.H., Bürgmann, R., Nadeau, R.M., Chen, T., Lapusta, N., 2010. Postseismic variations in seismic moment and recurrence interval of repeating earthquakes. Earth Planet. Sci. Lett. 299. https://doi.org/10.1016/j.epsl.2010.1008.1027.

Chen, K.H., Nadeau, R.M., Rau, R.-J., 2007. Towards a universal rule on the recurrence interval scaling of repeating earthquakes? Geophys. Res. Lett. 34. https://doi.org/10.1029/2007GL030554.

Chen, T., Lapusta, N., 2009. Scaling of small repeating earthquakes explained by interaction of seismic and aseismic slip in a rate and state fault model. J. Geophys. Res. 114. https://doi.org/10.1029/2008JB005749.

Chlieh, M., Avouac, J.P., Sieh, K., Natawidjaja, D.H., Galetzka, J., 2008. Heterogeneous coupling of the Sumatran megathrust constrained by geodetic and paleogeodetic measurements. J. Geophys. Res. 113. https://doi.org/10.1029/2007JB004981.

Collettini, C., Niemeijer, A., Viti, C., Marone, C., 2009. Fault zone fabric and fault weakness. Nature 462, 907–910. https://doi.org/10.1038/nature08585.

Collettini, C., Niemeijer, A., Viti, C., Smith, S.A.F., Marone, C., 2011. Fault structure, frictional properties and mixed-mode fault slip behavior. Earth Planet. Sci. Lett. 311, 316–327. https://doi.org/10.1016/j.epsl.2011.09.020.

d'Alessio, M.A., Williams, C., Bürgmann, R., 2006. Frictional strength heterogeneity and surface heat flow; implications for the strength of the creeping San Andreas fault. J. Geophys. Res. 111. https://doi.org/10.1029/2005JB003780.
Dieterich, J.H., 1979. Modeling of rock friction, I. Experimental results and constitutive equations. J. Geophys. Res. 84, 2161–2168.
Dmitrieva, K., Hotovec-Ellis, A.J., Prejean, S., Dunham, E.M., 2013. Frictional-faulting model for harmonic tremor before Redoubt Volcano eruptions. Nat. Geosci. 6, 652. https://doi.org/10.1038/ngeo1879.
Dominguez, L.A., Taira, T.A., Santoyo, M.A., 2016. Spatiotemporal variations of characteristic repeating earthquake sequences along the Middle America Trench in Mexico. J. Geophys. Res. 121, 8855–8870. https://doi.org/10.1002/2016JB013242.
Doubre, C., Peltzer, G., 2007. Fluid-controlled faulting process in the Asal Rift, Djibouti, from 8 yr of radar interferometry observations. Geology 35, 69.
Dragert, H., Kelin, W., James, T.S., 2001. A silent slip event on the deeper Cascadia subduction interface. Science 292, 1525–1528.
Duboeuf, L., De Barros, L., Cappa, F., Guglielmi, Y., Deschamps, A., Seguy, S., 2017. Aseismic motions drive a sparse seismicity during fluid injections into a fractured zone in a carbonate reservoir. J. Geophys. Res. https://doi.org/10.1002/2017JB014535.
Eberhart-Phillips, D., Bannister, S., 2015. 3-D imaging of the northern Hikurangi subduction zone, New Zealand: variations in subducted sediment, slab fluids and slow slip. Geophys. J. Int. 201, 838–855. https://doi.org/10.1093/gji/ggv057.
Fagereng, Å., den Hartog, S.A.M., 2017. Subduction megathrust creep governed by pressure solution and frictional-viscous flow. Nat. Geosci. 10, 51–57. https://doi.org/10.1038/ngeo2857.
Fagereng, Å., Harris, C., 2014. Interplay between fluid flow and fault–fracture mesh generation within underthrust sediments: geochemical evidence from the Chrystalls Beach Complex, New Zealand. Tectonophysics 612–613, 147–157. https://doi.org/10.1016/j.tecto.2013.12.002.
Fagereng, Å., Hillary, G.W.B., Diener, J.F.A., 2014. Brittle-viscous deformation, slow slip, and tremor. Geophys. Res. Lett. 41, 4159–4167. https://doi.org/10.1002/2014GL060433.
Fagereng, Å., Remitti, F., Sibson, R.H., 2010. Shear veins observed within anisotropic fabric at high angles to the maximum compressive stress. Nat. Geosci. 3, 482–485. https://doi.org/10.1038/NGEO898.
Fagereng, Å., Toy, V.G., 2011. Geology of the earthquake source: an introduction. Geol. Soc. (Lond.) Spec. Publ. 359, 1–16. https://doi.org/10.1144/SP359.1.
Faulkner, D.R., Sanchez-Roa, C., Boulton, C., Hartog, S.A.M., 2018. Pore fluid pressure development in compacting fault gouge in theory, experiments and nature. J. Geophys. Res. 123, 226–241. https://doi.org/10.1002/2017JB015130.
Feng, L., Hill, E.M., Elósegui, P., Qiu, Q., Hermawan, I., Banerjee, P., Sieh, K., 2015. Hunt for slow slip events along the Sumatran subduction zone in a decade of continuous GPS data. J. Geophys. Res., Solid Earth 120, 8623–8632. https://doi.org/10.1002/2015JB012503.
Field, E.H., Arrowsmith, R.J., Biasi, G.P., Bird, P., Dawson, T.E., Felzer, K.R., Jackson, D.D., Johnson, K.M., Jordan, T.H., Madden, C., Michael, A.J., Milner, K.R., Page, M.T., Parsons, T., Powers, P.M., Shaw, B.E., Thatcher, W.R., Weldon, R.J., Zeng, Y., 2014. Uniform California Earthquake Rupture Forecast, Version 3 (UCERF3)—the time-independent model. Bull. Seismol. Soc. Am. 104, 1122–1180. https://doi.org/10.1785/0120130164.
Freed, A.M., 2005. Earthquake triggering by static, dynamic, and postseismic stress transfer. Annu. Rev. Earth Planet. Sci. 33, 335–368.
Froment, B., McGuire, J.J., van der Hilst, R.D., Gouédard, P., Roland, E.C., Zhang, H., Collins, J.A., 2014. Imaging along-strike variations in mechanical properties of the Gofar transform fault, East Pacific Rise. J. Geophys. Res. 119, 7175–7194. https://doi.org/10.1002/2014JB011270.
Gao, X., Wang, K., 2014. Strength of stick-slip and creeping subduction megathrusts from heat flow observations. Science 345. https://doi.org/10.1126/science.1255487.
Gomberg, J., Wech, A., Creager, K., Obara, K., Agnew, D., 2016. Reconsidering earthquake scaling. Geophys. Res. Lett. 43. https://doi.org/10.1002/2016GL069967.
Guglielmi, Y., Cappa, F., Avouac, J.-P., Henry, P., Elsworth, D., 2015. Seismicity triggered by fluid injection-induced aseismic slip. Science 348, 1224–1226. https://doi.org/10.1126/science.aab0476.
Guilhem, A., Nadeau, R.M., 2012. Episodic tremors and deep slow-slip events in Central California. Earth Planet. Sci. Lett. 357, 1–10.
Handwerger, A.L., Rempel, A.W., Skarbek, R.M., Roering, J.J., Hilley, G.E., 2016. Rate-weakening friction characterizes both slow sliding and catastrophic failure of landslides. Proc. Natl. Acad. Sci. USA 113, 10281–10286.
Handy, M.R., Hirth, G., Bürgmann, R., 2007. Continental fault structure and rheology from the frictional-to-viscous transition downward. In: Handy, M.R., Hirth, G., Hovius, N. (Eds.), Tectonic Faults: Agents of Change on a Dynamic Earth. MIT Press, Cambridge, MA, pp. 139–181.
Harbord, C.W.A., Nielsen, S.B., De Paola, N., Holdsworth, R.E., 2017. Earthquake nucleation on rough faults. Geology 45, 931–934. https://doi.org/10.1130/G39181.1.
Hardebeck, J.L., Loveless, J.P., 2018. Creeping subduction zones are weaker than locked subduction zones. Nat. Geosci. 11, 60–64. https://doi.org/10.1038/s41561-017-0032-1.
Hardebeck, J.L., Michael, A.J., 2004. Stress orientations at intermediate angles to the San Andreas Fault, California. J. Geophys. Res. 109. https://doi.org/10.1029/2004JB003239.
Harris, R., Segall, P., 1987. Detection of a locked zone at depth on the Parkfield, California segment of the San Andreas fault. J. Geophys. Res. 92, 7945–7962.
Harris, R.A., 2017. Large earthquakes and creeping faults. Rev. Geophys. 55. https://doi.org/10.1002/2016RG000539.
Hatakeyama, N., Uchida, N., Matsuzawa, T., Nakamura, W., 2017. Emergence and disappearance of interplate repeating earthquakes following the 2011M9.0 Tohoku-oki earthquake: slip behavior transition between seismic and aseismic depending on the loading rate. J. Geophys. Res., Solid Earth 122. https://doi.org/10.1002/2016JB013914.
Hawthorne, J.C., Bartlow, N.M., 2018. Observing and modeling the spectrum of a slow slip event. J. Geophys. Res., Solid Earth 123. https://doi.org/10.1029/2017JB015124.
Hawthorne, J.C., Rubin, A.M., 2010. Tidal modulation of slow slip in Cascadia. J. Geophys. Res. 115. https://doi.org/10.1029/2010jb007502.
Hayman, N.W., Lavier, L.L., 2014. The geologic record of deep episodic tremor and slip. Geology 43, 223–226. https://doi.org/10.1130/G34990.1.
Hayward, T.W., Bostock, M.G., 2017. Slip behavior of the Queen Charlotte plate boundary before and after the 2012, MW 7.8 Haida Gwaii Earthquake: evidence from repeating earthquakes. J. Geophys. Res. 122, 8990–9011. https://doi.org/10.1002/2017JB014248.
He, C., Luo, L., Hao, Q.-M., Zhou, Y., 2013. Velocity-weakening behavior of plagioclase and pyroxene gouges and stabilizing effect of small amounts of quartz under hydrothermal conditions. J. Geophys. Res., Solid Earth 118, 3408–3430. https://doi.org/10.1002/jgrb.50280.
Hearn, E.H., Bürgmann, R., Reilinger, R., 2002. Dynamics of Izmit earthquake post-seismic deformation and loading of the Duzce earthquake hypocenter. Bull. Seismol. Soc. Am. 92, 172–193.
Heise, W., Caldwell, T.G., Bannister, S., Bertrand, E.A., Ogawa, Y., Bennie, S.L., Ichihara, H., 2017. Mapping subduction interface coupling using magnetotellurics; Hikurangi Margin, New Zealand. Geophys. Res. Lett. 44, 9261–9266. https://doi.org/10.1002/2017GL074641.
Hirose, J., Hirahara, K., Kimata, F., Fjii, N., Miyazaki, S., 1999. A slow thrust slip event following the two 1996 Hyuganada earthquakes beneath the Bongo Channel, southwest Japan. Geophys. Res. Lett. 26, 3237–3240.
Houston, H., 2015. Low friction and fault weakening revealed by rising sensitivity of tremor to tidal stress. Nat. Geosci. 8, 409–415. https://doi.org/10.1038/ngeo2419.
Hsu, Y.J., Simons, M., Avouac, J.P., Galetzka, J., Sieh, K., Chlieh, M., Natawidjaja, D., Prawirodirdjo, L., Bock, Y., 2006. Frictional afterslip following the 2005 Nias-Simeulue earthquake, Sumatra. Science 312. https://doi.org/10.1126/science.1136960.
Hu, Y., Bürgmann, R., Uchida, N., Banerjee, P., Freymueller, J.T., 2016. Stress-driven relaxation of heterogeneous upper mantle and time-dependent afterslip following the 2011 Tohoku earthquake. J. Geophys. Res. 121, 385–411. https://doi.org/10.1002/2015JB012508.
Ide, S., Beroza, G.C., Shelly, D.R., Uchide, T., 2007. A scaling law for slow earthquakes. Nature 447, 76–79. https://doi.org/10.1038/nature05780.
Ide, S., Maury, J., 2018. Seismic moment, seismic energy, and source duration of slow earthquakes: application of Brownian slow earthquake model to three major subduction zones. Geophys. Res. Lett. 45, 3059–3067. https://doi.org/10.1002/2018GL077461.
Ikari, M.J., Kopf, A.J., 2017. Seismic potential of weak, near-surface faults revealed at plate tectonic slip rates. Sci. Adv. 3 (11), e1701269. https://doi.org/10.1126/sciadv.1701269.
Ikari, M.J., Marone, C., Saffer, D.M., Kopf, A.J., 2013. Slip weakening as a mechanism for slow earthquakes. Nat. Geosci. 6, 468. https://doi.org/10.1038/ngeo1818.
Ikari, M.J., Saffer, D.M., Marone, C., 2009. Frictional and hydrologic properties of clay-rich fault gouge. J. Geophys. Res., Solid Earth 114. https://doi.org/10.1029/2008JB006089.
Ingleby, T., Wright, T.J., 2017. Omori-like decay of postseismic velocities following continental earthquakes. Geophys. Res. Lett. 44, 3119–3130. https://doi.org/10.1002/2017GL072865.
Ito, Y., Obara, K., Shiomi, K., Sekine, S., Hirose, H., 2007. Slow earthquakes coincident with episodic tremors and slow slip events. Science 315, 503–506. https://doi.org/10.1126/science.1134454.
Johnson, K.M., Shelly, D.R., Bradley, A.M., 2013. Simulations of tremor-related creep reveal a weak crustal root of the San Andreas Fault. Geophys. Res. Lett. 40, 1300–1305. https://doi.org/10.1002/grl.50216.
Jolivet, R., Lasserre, C., Doin, M.P., Guillaso, S., Peltzer, G., Dailu, R., Sun, J., Shen, Z.K., Xu, X., 2012. Shallow creep on the Haiyuan Fault (Gansu, China) revealed by SAR, interferometry. J. Geophys. Res. 117, B06401. https://doi.org/10.1029/2011jb008732.
Jolivet, R., Simons, M., Agram, P.S., Duputel, Z., Shen, Z.-K., 2015. Aseismic slip and seismogenic coupling along the central San Andreas Fault. Geophys. Res. Lett. 42, 297–306. https://doi.org/10.1002/2014GL062222.
Kaduri, M., Gratier, J.-P., Renard, F., Çakir, Z., Lasserre, C., 2017. The implications of fault zone transformation on aseismic creep: example of the North Anatolian Fault, Turkey. J. Geophys. Res. 122, 4208–4236. https://doi.org/10.1002/2016JB013803.

Kaproth, B.M., Marone, C., 2013. Slow earthquakes, preseismic velocity changes, and the origin of slow frictional stick–slip. Science 341, 1229–1232. https://doi.org/10.1126/science.1239577.

Kato, A., Obara, K., Igarashi, T., Tsuruoka, H., Nakagawa, S., Hirata, N., 2012. Propagation of slow slip leading up to the 2011 Mw 9.0 Tohoku–Oki earthquake. Science 335. https://doi.org/10.1126/science.1215141.

Kodaira, S., Iidaka, T., Kato, A., Park, J.O., Iwasaki, T., Kaneda, Y., 2004. High pore fluid pressure may cause silent slip in the Nankai Trough. Science 304, 1295–1298. https://doi.org/10.1126/science.1096535.

Kohli, A.H., Goldsby, D.L., Hirth, G., Tullis, T.E., 2011. Flash weakening of serpentinite at near-seismic slip rates. J. Geophys. Res., Solid Earth 116. https://doi.org/10.1029/2010JB007833.

Lavier, L.L., Bennett, R.A., Duddu, R., 2013. Creep events at the brittle ductile transition. Geochem. Geophys. Geosyst. 14, 3334–3351. https://doi.org/10.1002/ggge.20178.

Lay, T., Kanamori, H., Ammon, C.J., Koper, K.D., Hutko, A.R., Ye, L., Yue, H., Rushing, T.M., 2012. Depth-varying rupture properties of subduction zone megathrust faults. J. Geophys. Res. 117 (B4), B04311. https://doi.org/10.1029/2011jb009133.

Leeman, J.R., Saffer, D.M., Scuderi, M.M., Marone, C., 2016. Laboratory observations of slow earthquakes and the spectrum of tectonic fault slip modes. Nat. Commun. 7, 11104. https://doi.org/10.1038/ncomms11104.

Lewis, M.A., Ben-Zion, Y., 2010. Diversity of fault zone damage and trapping structures in the Parkfield section of the San Andreas Fault from comprehensive analysis of near fault seismograms. Geophys. J. Int. 183, 1579–1595. https://doi.org/10.1111/j.1365-246X.2010.04816.x.

Lewis, M.A., Ben-Zion, Y., McGuire, J.J., 2007. Imaging the deep structure of the San Andreas Fault south of Hollister with joint analysis of fault zone head and direct P arrivals. Geophys. J. Int. 169, 1028–1042. https://doi.org/10.1111/j.1365-246X.2006.03319.x.

Li, Y.-G., Ellsworth, W., Thurber, C., Malin, P., Aki, K., 1997. Fault-zone guided waves from explosions in the San Andreas fault in Parkfield and Cienega Valley California. Bull. Seismol. Soc. Am. 87, 210–221.

Lienkaemper, J.J., McFarland, F.S., Simpson, R.W., Caskey, S.J., 2014. Using surface creep rate to infer fraction locked for sections of the San Andreas Fault System in Northern California from alignment array and GPS data. Bull. Seismol. Soc. Am. 104. https://doi.org/10.1785/0120140117.

Linde, A.T., Gladwin, M.T., Johnston, M.J.S., Gwyther, R.L., Bilham, R.G., 1996. A slow earthquake sequence on the San Andreas fault. Nature 383, 65–68.

Lipovsky, B.P., Dunham, E.M., 2017. Slow-slip events on the Whillans Ice Plain, Antarctica, described using rate-and-state friction as an ice stream sliding law. J. Geophys. Res., Earth Surf. 122, 973–1003. https://doi.org/10.1002/2016JF004183.

Liu, Y., Rice, J.R., 2009. Slow slip predictions based on granite and gabbro friction data compared to GPS measurements in northern Cascadia. J. Geophys. Res., Solid Earth 114. https://doi.org/10.1029/2008JB006142.

Lockner, D.A., Morrow, C., Moore, D., Hickman, S., 2011. Low strength of deep San Andreas fault gouge from SAFOD core. Nature 472, 82–85. https://doi.org/10.1038/nature09927.

Lohman, R.B., McGuire, J.J., 2007. Earthquake swarms driven by aseismic creep in the Salton Trough, California. J. Geophys. Res. 112. https://doi.org/10.1029/2006jb004596. https://doi.org/10.1029/2006jb004596.

Louderback, G.D., 1942. Faults and earthquakes. Bull. Seismol. Soc. Am. 32, 305–330.

Loveless, J.P., Meade, B., 2011. Spatial correlation of interseismic coupling and coseismic rupture extent of the 2011 Mw = 9.0 Tohoku-oki earthquake. Geophys. Res. Lett. 38. https://doi.org/10.1029/2011GL048561.

Marone, C.J., 1998. Laboratory-derived friction laws and their application to seismic faulting. Annu. Rev. Earth Planet. Sci. 26, 643–696.

Materna, K., Taira, T., Bürgmann, R., 2018. Aseismic transform fault slip at the Mendocino Triple Junction from characteristically repeating earthquakes. Geophys. Res. Lett. 45. https://doi.org/10.1002/2017GL075899.

Mavrommatis, A.P., Segall, P., Uchida, N., Johnson, K.M., 2015. Long-term acceleration of aseismic slip preceding the Mw 9 Tohoku-oki earthquake: constraints from repeating earthquakes. Geophys. Res. Lett. 42. https://doi.org/10.1002/2015GL066069.

Mazzotti, S., Adams, J., 2004. Variability of nearterm probability for the next great earthquake on the Cascadia subduction zone. Bull. Seismol. Soc. Am. 94. https://doi.org/10.1785/012004032.

McGuire, J.J., Collins, J.A., Gouedard, P., Roland, E., Lizarralde, D., Boettcher, M.S., Behn, M.D., van der Hilst, R.D., 2012. Variations in earthquake rupture properties along the Gofar transform fault, East Pacific Rise. Nat. Geosci. 5, 336–341. https://doi.org/10.1038/ngeo1454.

McGuire, J.J., Plank, T., et al., 2017. The SZ4D Initiative: Understanding the Processes that Underlie Subduction Zone Hazards in 4D. Vision document submitted to the National Science Foundation. The IRIS Consortium. 63 pp. http://www.iris.edu/hq/files/workshops/2016/2009/szo_2016/sz2014d.pdf.

McLaskey, G.C., Kilgore, B.D., 2013. Foreshocks during the nucleation of stick-slip instability. J. Geophys. Res., Solid Earth 118, 2982–2997. https://doi.org/10.1002/jgrb.50232.

McLaskey, G.C., Yamashita, F., 2017. Slow and fast ruptures on a laboratory fault controlled by loading characteristics. J. Geophys. Res., Solid Earth 122. https://doi.org/10.1002/2016JB013681.

Meade, B.J., Loveless, J.P., 2009. Predicting the geodetic signature of Mw ≥ 8 slow slip events. Geophys. Res. Lett. 36. https://doi.org/10.1029/2008GL036364.

Meneghini, F., Moore, J.C., 2007. Deformation and hydrofracture in a subduction thrust at seismogenic depths: the Rodeo Cove thrust zone, Marin Headlands, California. Geol. Soc. Am. Bull. 119, 174–183. https://doi.org/10.1130/B25807.1.

Meng, L., Huang, H., Bürgmann, R., Ampuero, J.-P., Strader, A., 2015. Dual megathrust slip behaviors of the 2014 Iquique Earthquake sequence. Earth Planet. Sci. Lett. 411, 177–187. https://doi.org/10.1016/j.epsl.2014.11.041.

Montesi, L.G.J., 2004. Controls of shear zone rheology and tectonic loading on postseismic creep. J. Geophys. Res. 109. https://doi.org/10.1029/JB2003JB002925.

Moore, D.E., Rymer, M.J., 2007. Talc-bearing serpentinite and the creeping section of the San Andreas fault. Nature 448, 795–797. https://doi.org/10.1038/nature06064.

Nadeau, R.M., Johnson, L.R., 1998. Seismological studies at Parkfield VI: moment release rates and estimates of source parameters for small repeating earthquakes. Bull. Seismol. Soc. Am. 88, 790–814.

Nadeau, R.M., McEvilly, T.V., 1999. Fault slip rates at depth from recurrence intervals of repeating microearthquakes. Science 285, 718–721.

Nedimovic, M.R., Hyndman, R.D., Ramachandran, K., Spence, G.D., 2003. Reflection signature of seismic and aseismic slip on the northern Cascadia subduction interface. Nature 424, 416–420.

Niemeijer, A.R., Spiers, C.J., 2006. Velocity dependence of strength and healing behaviour in simulated phyllosilicate-bearing fault gouge. Tectonophysics 427, 231–253. https://doi.org/10.1016/j.tecto.2006.03.048.

Nishikawa, T., Ide, S., 2017. Detection of earthquake swarms at subduction zones globally: insights into tectonic controls on swarm activity. J. Geophys. Res., Solid Earth 122. https://doi.org/10.1002/2017JB014188.

Nishimura, T., Matsuzawa, T., Obara, K., 2013. Detection of short-term slow slip events along the Nankai Trough, southwest Japan, using GNSS data. J. Geophys. Res., Solid Earth 118. https://doi.org/10.1002/jgrb.50222.

Noda, H., Lapusta, N., 2013. Stable creeping fault segments can become destructive as a result of dynamic weakening. Nature 493, 518. https://doi.org/10.1038/nature11703.

Obara, K., 2002. Nonvolcanic deep tremor associated with subduction in Southwest Japan. Science 296, 1679–1681. https://doi.org/10.1126/science.1070378.

Obara, K., Kato, A., 2016. Connecting slow earthquakes to huge earthquakes. Science 353, 253–257. https://doi.org/10.1126/science.aaf1512.

Ohta, Y., Freymueller, J., Hreinsdottir, S., Suito, H., 2006. A large slow slip event and the depth of the seismogenic zone in the south central Alaska subduction zone. Earth Planet. Sci. Lett. 247, 108–116. https://doi.org/10.1016/j.epsl.2006.05.013.

Outerbridge, K.C., Dixon, T.H., Schwartz, S.Y., Walter, J.I., Protti, M., Gonzalez, V., Biggs, J., Thorwart, M., Rabbel, W., 2010. A tremor and slip event on the Cocos-Caribbean subduction zone as measured by a global positioning system (GPS) and seismic network on the Nicoya Peninsula, Costa Rica. J. Geophys. Res., Solid Earth 115. https://doi.org/10.1029/2009JB006845.

Pec, M., Stünitz, H., Heilbronner, R., Drury, M., 2016. Semi-brittle flow of granitoid fault rocks in experiments. J. Geophys. Res. 121, 1677–1705. https://doi.org/10.1002/2015JB012513.

Peng, Z., Ben-Zion, Y., 2005. Spatiotemporal variations of crustal anisotropy from similar events in aftershocks of the 1999 M7.4 İzmit and M7.1 Düzce, Turkey, earthquake sequences. Geophys. J. Int. 160, 1027–1043. https://doi.org/10.1111/j.1365-246X.2005.02569.x.

Peng, Z., Gomberg, J., 2010. An integrated perspective of the continuum between earthquakes and slow-slip phenomena. Nat. Geosci. 3. https://doi.org/10.1038/ngeo940.

Pousse Beltran, L., Pathier, E., Jouanne, F., Vassallo, R., Reinoza, C., Audemard, F., Doin, M.P., Volat, M., 2016. Spatial and temporal variations in creep rate along the El Pilar fault at the Caribbean–South American plate boundary (Venezuela) from InSAR. J. Geophys. Res. 121, 8276–8296. https://doi.org/10.1002/2016JB013121.

Radiguet, M., Cotton, F., Vergnolle, M., Campillo, M., Walpersdorf, A., Cotte, N., Kostoglodov, V., 2012. Slow slip events and strain accumulation in the Guerrero gap, Mexico. J. Geophys. Res., Solid Earth 117. https://doi.org/10.1029/2011JB008801.

Radiguet, M., Perfettini, H., Cotte, N., Gualandi, A., Valette, B., Kostoglodov, V., Lhomme, T., Walpersdorf, A., Cabral Cano, E., Campillo, M., 2016. Triggering of the 2014 Mw7.3 Papanoa earthquake by a slow slip event in Guerrero, Mexico. Nat. Geosci. 9, 829–833. https://doi.org/10.1038/ngeo2817.

Reber, J.E., Lavier, L.L., Hayman, N.W., 2015. Experimental demonstration of a semi-brittle origin for crustal strain transients. Nat. Geosci. 8, 712–715. https://doi.org/10.1038/NGEO2496.

Richard, J., Gratier, J.-P., Doan, M.-L., Boullier, A.-M., Renard, F., 2014. Rock and mineral transformations in a fault zone leading to permanent creep: interactions between brittle and viscous mechanisms in the San Andreas Fault. J. Geophys. Res. 119, 8132–8153. https://doi.org/10.1002/2014JB011489.

Roeloffs, E.A., 2006. Evidence for aseismic deformation rate changes prior to earthquakes. Annu. Rev. Earth Planet. Sci. 35, 591–627. https://doi.org/10.1146/annurev.earth.34.031405.124947.

Rogers, G., Dragert, H., 2003. Episodic tremor and slip on the Cascadia subduction zone: the chatter of silent slip. Science 300, 1942–1943. https://doi.org/10.1126/science.1084783.

Roland, E., Lizarralde, D., McGuire, J.J., Collins, J.A., 2012. Seismic velocity constraints on the material properties that control earthquake behavior at the Quebrada-Discovery-Gofar transform faults, East Pacific Rise. J. Geophys. Res., Solid Earth 117. https://doi.org/10.1029/2012JB009422.

Roland, E., McGuire, J.J., 2009. Earthquake swarms on transform faults. Geophys. J. Int. 178, 1677–1690. https://doi.org/10.1111/j.1365-246X.2009.04214.x.

Rolandone, F., Nocquet, J.-M., Mothes, P.A., Jarrin, P., Vallée, M., Cubas, N., Hernandez, S., Plain, M., Vaca, S., Font, Y., 2018. Areas prone to slow slip events impede earthquake rupture propagation and promote afterslip. Sci. Adv. 4.

Rousset, B., Jolivet, R., Simons, M., Lasserre, C., Riel, B., Milillo, P., Çakir, Z., Renard, F., 2016. An aseismic slip transient on the North Anatolian Fault. Geophys. Res. Lett. 43, 3254–3262. https://doi.org/10.1002/2016GL068250.

Rowe, C.D., Griffith, W.A., 2015. Do faults preserve a record of seismic slip: a second opinion. J. Struct. Geol. 78, 1–26. https://doi.org/10.1016/j.jsg.2015.06.006.

Rowe, C.D., Meneghini, F., Moore, J.C., 2011. Textural record of the seismic cycle: strain-rate variation in an ancient subduction thrust. Geol. Soc. (Lond.) Spec. Publ. 359, 77–95. https://doi.org/10.1144/SP359.5.

Rowe, C.D., Moore, J.C., Remitti, F., 2013. The thickness of subduction plate boundary faults from the seafloor into the seismogenic zone. Geology 41, 991–994. https://doi.org/10.1130/G34556.1.

Rubinstein, J.L., Ellsworth, W.L., Chen, K.H., Uchida, N., 2012. Fixed recurrence and slip models better predict earthquake behavior than the time- and slip-predictable models: 1. Repeating earthquakes. J. Geophys. Res., Solid Earth 117. https://doi.org/10.1029/2011JB008724.

Rubinstein, J.L., Shelly, D.R., Ellsworth, W.L., 2010. Non-volcanic tremor: a window into the roots of fault zones. In: Cloetingh, S., Negendank, J. (Eds.), New Frontiers in Integrated Solid Earth Sciences. Springer Netherlands, Dordrecht, pp. 287–314.

Saffer, D.M., 2017. Mapping fluids to subduction megathrust locking and slip behavior. Geophys. Res. Lett. 44, 9337–9340. https://doi.org/10.1002/2017GL075381.

Saffer, D.M., Lockner, D.A., McKiernan, A., 2012. Effects of smectite to illite transformation on the frictional strength and sliding stability of intact marine mudstones. Geophys. Res. Lett. 39. https://doi.org/10.1029/2012GL051761.

Saffer, D.M., Wallace, L.M., 2015. The frictional, hydrologic, metamorphic and thermal habitat of shallow slow earthquakes. Nat. Geosci. 8, 594–600. https://doi.org/10.1038/ngeo2490.

Saito, T., Ujiie, K., Tsutsumi, A., Kameda, J., Shibazaki, B., 2013. Geological and frictional aspects of very-low-frequency earthquakes in an accretionary prism. Geophys. Res. Lett. 40, 703–708. https://doi.org/10.1002/grl.50175.

Savage, J.C., Burford, R.O., 1970. Accumulation of tectonic strain in California. Bull. Seismol. Soc. Am. 60, 1877–1896.

Schwartz, S.Y., 2015. Episodic aseismic slip at plate boundaries. In: Schubert, Gerald (Ed.), Treatise on Geophysics, second edition. Elsevier, Oxford, pp. 445–465.

Schwartz, S.Y., Rokosky, J.M., 2007. Slow slip events and seismic tremor at circum-Pacific subduction zones. Rev. Geophys. 45. https://doi.org/10.1029/2006rg000208.

Scuderi, M.M., Collettini, C., Marone, C., 2017. Frictional stability and earthquake triggering during fluid pressure stimulation of an experimental fault. Earth Planet. Sci. Lett. 477, 84–96. https://doi.org/10.1016/j.epsl.2017.08.009.

Segall, P., Bradley, A.M., 2012. Slow-slip evolves into megathrust earthquakes in 2D numerical simulations. Geophys. Res. Lett. 39. https://doi.org/10.1029/2012GL052811.

Segall, P., Rubin, A.M., Bradley, A.M., Rice, J.R., 2010. Dilatant strengthening as a mechanism for slow slip events. J. Geophys. Res. 115. https://doi.org/10.1029/2010JB007449.

Shelly, D.R., 2017a. A 15 year catalog of more than 1 million low-frequency earthquakes: tracking tremor and slip along the deep San Andreas Fault. J. Geophys. Res. 122, 3739–3753. https://doi.org/10.1002/2017JB014047.

Shelly, D.R., 2017b. A 15 year catalog of more than 1 million low-frequency earthquakes: tracking tremor and slip along the deep San Andreas Fault. J. Geophys. Res., Solid Earth 122, 3739–3753. https://doi.org/10.1002/2017JB014047.

Shelly, D.R., Beroza, G.C., Ide, S., Nakamula, S., 2006. Low-frequency earthquakes in Shikoku, Japan, and their relationship to episodic tremor and slip. Nature 442, 188–191.

Shibazaki, B., Matsuzawa, T., Tsutsumi, A., Ujiie, K., Hasegawa, A., Ito, Y., 2011. 3D modeling of the cycle of a great Tohoku-oki earthquake, considering frictional behavior at low to high slip velocities. Geophys. Res. Lett. 38. https://doi.org/10.1029/2011GL049308.

Shimamoto, T., Noda, H., 2014. A friction to flow constitutive law and its application to a 2-D modeling of earthquakes. J. Geophys. Res., Solid Earth 119, 8089–8106. https://doi.org/10.1002/2014JB011170.

Shirzaei, M., Bürgmann, R., 2013. Time-dependent model of creep on the Hayward fault from joint inversion of 18 years of InSAR and surface creep data. J. Geophys. Res. 118. https://doi.org/10.1002/jgrb.50149.

Shirzaei, M., Bürgmann, R., Uchida, N., Hu, Y., Pollitz, F., Matsuzawa, T., 2014. Seismic versus aseismic slip: probing mechanical properties of the northeast Japan subduction zone. Earth Planet. Sci. Lett. 406, 7–13. https://doi.org/10.1016/j.epsl.2014.08.035.

Shirzaei, M., Taira, T., Bürgmann, R., 2013. Implications of recent asperity failures and aseismic creep for time-dependent earthquake hazard on the Hayward fault. Earth Planet. Sci. Lett. 371–372, 59–66. https://doi.org/10.1016/j.epsl.2013.04.024.

Sibson, R., 1977. Faults rocks and fault mechanisms. J. Geol. Soc. (Lond.) 133, 191–213. https://doi.org/10.1144/gsjgs.133.3.0191.

Sibson, R.H., 1982. Fault zone models, heat flow, and the depth distribution of earthquakes in the continental crust of the United States. Bull. Seismol. Soc. Am. 72, 151–163.

Sibson, R.H., 1989. Earthquake faulting as a structural process. J. Struct. Geol. 11, 1–14.

Sibson, R.H., 2017. Tensile overpressure compartments on low-angle thrust faults. Earth Planets Space 69, 113. https://doi.org/10.1186/s40623-017-0699-y.

Skarbek, R.M., Rempel, A.W., Schmidt, D.A., 2012. Geologic heterogeneity can produce aseismic slip transients. Geophys. Res. Lett. 39. https://doi.org/10.1029/2012GL053762.

Socquet, A., Valdes, J.P., Jara, J., Cotton, F., Walpersdorf, A., Cotte, N., Specht, S., Ortega-Culaciati, F., Carrizo, D., Norabuena, E., 2017. An 8 month slow slip event triggers progressive nucleation of the 2014 Chile megathrust. Geophys. Res. Lett. 44, 4046–4053. https://doi.org/10.1002/2017GL073023.

Steinbrugge, K.V., Zacher, E.G., Tocher, D., Whitten, C.A., Claire, C.N., 1960. Creep on the San Andreas fault. Bull. Seismol. Soc. Am. 50, 389–415.

Taira, T., Bürgmann, R., Nadeau, R.M., Dreger, D.D., 2014. Variability of fault slip behavior along the San Andreas Fault in the San Juan Bautista Region. J. Geophys. Res. 119. https://doi.org/10.1002/2014JB011427.

Thomas, A.M., Beeler, N.M., Bletery, Q., Bürgmann, R., Shelly, D.R., 2018. Using low frequency earthquake families on the San Andreas fault as deep creepmeters. J. Geophys. Res., Solid Earth 123. https://doi.org/10.1002/2017JB014404.

Thomas, A.M., Bürgmann, R., Shelly, D.R., Beeler, N.M., Rudolph, M.L., 2012. Tidal triggering of low frequency earthquakes near Parkfield, CA: implications for fault mechanics within the brittle–ductile transition. J. Geophys. Res. 117. https://doi.org/10.1029/2011JB009036.

Thomas, M.Y., Avouac, J.-P., Champenois, J., Lee, J.-C., Kuo, L.-C., 2014a. Spatiotemporal evolution of seismic and aseismic slip on the Longitudinal Valley Fault, Taiwan. J. Geophys. Res., Solid Earth 119. https://doi.org/10.1002/2013JB010603.

Thomas, M.Y., Avouac, J.-P., Gratier, J.-P., Lee, J.-C., 2014b. Lithological control on the deformation mechanism and the mode of fault slip on the Longitudinal Valley Fault, Taiwan. Tectonophysics 632, 48–63. https://doi.org/10.1016/j.tecto.2014.05.038.

Thurber, C., Roecker, S., Ellsworth, W., Chen, Y., Lutter, W., Sessions, R., 1997. Two-dimensional seismic image of the San Andreas Fault in the Northern Gabilan Range, central California: evidence for fluids in the fault zone. Geophys. Res. Lett. 24, 1591–1594.

Tobin, H.J., Saffer, D.M., 2009. Elevated fluid pressure and extreme mechanical weakness of a plate boundary thrust, Nankai Trough subduction zone. Geology 37, 679–682. https://doi.org/10.1130/G25752A.1.

Tsang, L.L.H., Meltzner, A.J., Philibosian, B., Hill, E.M., Freymueller, J.T., Sieh, K., 2015. A 15 year slow-slip event on the Sunda megathrust offshore Sumatra. Geophys. Res. Lett. 42, 6630–6638. https://doi.org/10.1002/2015GL064928.

Turner, R.C., Shirzaei, M., Nadeau, R.M., Bürgmann, R., 2015. Slow and go: pulsing slip rates on the creeping section of the San Andreas Fault. J. Geophys. Res. 120. https://doi.org/10.1002/2015JB011998.

Uchida, N., Iinuma, T., Nadeau, R.M., Bürgmann, R., Hino, R., 2016. Periodic slow slip triggers megathrust zone earthquakes in northeastern Japan. Science 351, 488–492. https://doi.org/10.1126/science.aad3108.

Uchida, N., Matsuzawa, T., 2013. Pre- and postseismic slow slip surrounding the 2011 Tohoku-oki earthquake rupture. Earth Planet. Sci. Lett. 374, 81–91. https://doi.org/10.1016/j.epsl.2013.05.021.

Valoroso, L., Chiaraluce, L., Di Stefano, R., Monachesi, G., 2017. Mixed-mode slip behavior of the Altotiberina low-angle normal fault system (Northern Apennines, Italy) through high-resolution earthquake locations and repeating events. J. Geophys. Res. 122, 10220–210240. https://doi.org/10.1002/2017JB014607.

Veedu, D.M., Barbot, S., 2016. The Parkfield tremors reveal slow and fast ruptures on the same asperity. Nature 532, 361. https://doi.org/10.1038/nature17190.

Vidale, J.E., Shearer, P.M., 2006. A survey of 71 earthquake bursts across southern California: exploring the role of pore fluid pressure fluctuations and aseismic slip as drivers. J. Geophys. Res., Solid Earth 111. https://doi.org/10.1029/2005JB004034.

Vuan, A., Sugan, M., Chiaraluce, L., Di Stefano, R., 2017. Loading rate variations along a midcrustal shear zone the Mw6.0 earthquake of 24 August 2016 in Central Italy. Geophys. Res. Lett. 44. https://doi.org/10.1002/2017GL076223.

Wallace, L.M., Kaneko, Y., Hreinsdottir, S., Hamling, I., Peng, Z., Bartlow, N., D'Anastasio, E., Fry, B., 2017. Large-scale dynamic triggering of shallow slow slip enhanced by overlying sedimentary wedge. Nat. Geosci. 10, 765–770. https://doi.org/10.1038/ngeo3021.

Wallace, L.M., Webb, S.C., Ito, Y., Mochizuki, K., Hino, R., Henrys, S., Schwartz, S.Y., Sheehan, A.F., 2016. Slow slip near the trench at the Hikurangi subduction zone, New Zealand. Science 352, 701.

Wang, K., Bilek, S.L., 2014. Invited review paper: fault creep caused by subduction of rough seafloor relief. Tectonophysics 610, 1–24. https://doi.org/10.1016/j.tecto.2013.11.024.

Wang, K., Dixon, T.H., 2004. "Coupling" semantics and science in earthquake research. Eos 85, 180.

Wannamaker, P.E., Evans, R.L., Bedrosian, P.A., Unsworth, M.J., Maris, V., McGary, R.S., 2014. Segmentation of plate coupling, fate of subduction fluids, and modes of arc magmatism in Cascadia, inferred from magnetotelluric resistivity. Geochem. Geophys. Geosyst. 15, 4230–4253. https://doi.org/10.1002/2014GC005509.

Wech, A., 2016. Extending Alaska's plate boundary: tectonic tremor generated by Yakutat subduction. Geology 44, 587–590. https://doi.org/10.1130/G37817.1.

Wech, A.G., Bartlow, N.M., 2014. Slip rate and tremor genesis in Cascadia. Geophys. Res. Lett. 41, 392–398. https://doi.org/10.1002/2013GL058607.

Yao, D., Walter, J.I., Meng, X., Hobbs, T.E., Peng, Z., Newman, A.V., Schwartz, S.Y., Protti, M., 2017. Detailed spatiotemporal evolution of microseismicity and repeating earthquakes following the 2012 Mw 7.6 Nicoya earthquake. J. Geophys. Res. 122, 524–542. https://doi.org/10.1002/2016JB013632.

Yin, A., Xie, Z., Meng, L., 2018. A viscoplastic model for deep (15–50 km) slow-slip events at plate convergent margins. Earth Planet. Sci. Lett. 491, 81–94. https://doi.org/10.1016/j.epsl.2018.02.042.

Yokota, Y., Ishikawa, T., Watanabe, S., Tashiro, T., Asada, A., 2016. Seafloor geodetic constraints on interplate coupling of the Nankai Trough megathrust zone. Nature 534, 374–377. https://doi.org/10.1038/nature17632.

Zeng, X., Thurber, C.H., Shelly, D.R., Harrington, R.M., Cochran, E.S., Bennington, N.L., Peterson, D., Guo, B., McClement, K., 2016. 3-D P- and S-wave velocity structure and low-frequency earthquake locations in the Parkfield, California region. Geophys. J. Int. 206, 1574–1585. https://doi.org/10.1093/gji/ggw217.

Zhao, D., Huang, Z., Umino, N., Hasegawa, A., Kanamori, H., 2011. Structural heterogeneity in the megathrust zone and mechanism of the 2011 Tohoku-oki earthquake (Mw 9.0). Geophys. Res. Lett. 38. https://doi.org/10.1029/2011GL048408.

Zoback, M.D., Hickman, S.H., Ellsworth, W.L., 2010. Scientific drilling into the San Andreas fault zone. Eos Trans. AGU 91, 197–199. https://doi.org/10.1029/2010EO220001.

Zoback, M.D., Kohli, A., Das, I., McClure, M.W., 2012. The Importance of Slow Slip on Faults During Hydraulic Fracturing Stimulation of Shale Gas Reservoirs. Society of Petroleum Engineers.